Mode-coupling theory for active Brownian particles

Alexander Liluashvili,[1] Jonathan Ónody,[1] and Thomas Voigtmann[1,2]
[1]*Institut für Materialphysik im Weltraum, Deutsches Zentrum für Luft- und Raumfahrt, 51170 Köln, Germany*
[2]*Department of Physics, Heinrich-Heine Universität Düsseldorf, Universitätsstraße 1, 40225 Düsseldorf, Germany*
(Received 8 August 2017; published 14 December 2017)

We present a mode-coupling theory (MCT) for the slow dynamics of two-dimensional spherical active Brownian particles (ABPs). The ABPs are characterized by a self-propulsion velocity v_0 and by their translational and rotational diffusion coefficients D_t and D_r, respectively. Based on the integration-through-transients formalism, the theory requires as input only the equilibrium static structure factors of the passive system (where $v_0 = 0$). It predicts a nontrivial idealized-glass-transition diagram in the three-dimensional parameter space of density, self-propulsion velocity, and rotational diffusivity that arise because at high densities, the persistence length of active swimming $\ell_p = v_0/D_r$ interferes with the interaction length ℓ_c set by the caging of particles. While the low-density dynamics of ABPs is characterized by a single Péclet number $\mathrm{Pe} = v_0^2/D_r D_t$, close to the glass transition the dynamics is found to depend on Pe and ℓ_p separately. At fixed density, increasing the self-propulsion velocity causes structural relaxation to speed up, while decreasing the persistence length slows down the relaxation. The active-MCT glass is a nonergodic state that is qualitatively different from the passive glass. In it, correlations of initial density fluctuations never fully decay, but also an infinite memory of initial orientational fluctuations is retained in the positions.

DOI: 10.1103/PhysRevE.96.062608

I. INTRODUCTION

The collective dynamics of self-propelled particles and the related behavior of dense suspensions of microswimmers have received an increasing amount of attention in the past few years. The physical principles of this dynamics are relevant for many biophysical questions. For example, mechanisms at work in wound healing (tissue repair) have been likened to the collective dynamics found in model microswimmer systems [1–6]. The collective dynamics of cells, bacteria colonies, or that found in the cell cytoskeleton show slow dynamics. It can be associated with the slow dynamics that arises from crowding effects at high densities and from the approach to a glass or jamming transition [7–13].

Colloidal self-propelled particles provide paradigmatic model systems to study the qualitative effects of swimming and generic features of a broad class of intrinsically nonequilibrium matter. In experiment, suspensions of self-phoretic Brownian particles are a good realization of this model. Half-capped Janus particles offer a surface-mediated mechanism to convert energy provided by light fields or chemical fuel into directed motion, superimposed on the Brownian translational and rotational diffusion of passive colloids [14–19].

One of the simplest theoretical models in this context is that of active Brownian particles (ABPs) [20,21]. These are orientable colloidal particles that undergo passive translational and rotational Brownian motion and in addition an active drift along a body-fixed orientation axis due to intrinsic self-propulsion forces. In two spatial dimensions, particles are described by their positions $\vec{r}_i$ and orientation angles θ_i with respect to a fixed direction in space. Here $i = 1, \ldots N$ labels the particles. The equations of motion read, in the case of spherically symmetric interaction forces,

$$d\vec{r}_i = \vec{F}_i/\zeta\, dt + \sqrt{2D_t}\, d\vec{W}_i + v_0\vec{o}(\theta_i)dt, \tag{1a}$$

$$d\theta_i = \sqrt{2D_r}\, dW_{\theta_i}, \tag{1b}$$

where $\vec{o}(\theta) = (\cos\theta, \sin\theta)^T$ is the orientation vector. We will abbreviate $\vec{o}_i = \vec{o}(\theta_i)$. The elements of dW are independent Wiener processes and the $\vec{F}_i$ are the interaction forces. The friction coefficient $\zeta = 1/\beta D_t$ is taken to obey the fluctuation-dissipation theorem for the translational Brownian motion of the passive-particle system, with inverse temperature β. The key parameters characterizing the dynamics of a single spherical ABP are D_t, D_r, and v_0, the translational short-time diffusion coefficient, the rotational diffusion coefficient, and the self-propulsion velocity, respectively. Although for a passive colloid D_r and D_t are coupled due to the hydrodynamics of the solvent, for spherical ABPs it makes sense to treat D_r as an independent model parameter. Different self-propulsion mechanisms impose different persistence effects on the orientation that can be captured by varying the persistence time $1/D_r$ [22].

We focus on spherical ABPs with strongly repulsive interactions. The steric interactions are modeled by the equilibrium structure of a hard-sphere suspension and we ignore hydrodynamic interactions between the particles. At high densities, such systems (with suitable size polydispersity) are known from simulation to form glasses [23–25], as do related active-particle models [6,21,26–30].

The ABP model is a clean and therefore paradigmatic model where nonequilibrium forces couple the rotational to the translational degrees of freedom. Theoretical treatments of the collective dynamics so far proceed by various approximations that amount to coarse graining or integrating out the rotational degrees of freedom with various levels of accuracy. In this paper, we develop a theory to describe the glass transition and the dynamics in its vicinity, which resolves both positional-density and orientational fluctuations and thus takes the coupling in Eqs. (1) seriously, as one should do, so we argue, at high densities. Furthermore, the theory that we present here can be evaluated using as input quantities only the well-known structure functions of the passive-equilibrium high-density system.

At low and moderate densities the ABP model has been extensively studied (see, e.g., Refs. [31–47]). An effective-diffusion limit can be performed at large time scales $D_r t \gg 1$ to map the dynamics of the dilute system onto Brownian motion with an effective-diffusion coefficient $D_{\rm eff} = D_t + D_{\rm act} = D_t(1 + {\rm Pe}/2)$, where ${\rm Pe} = v_0^2/D_r D_t$ defines the relevant Péclet number and $D_{\rm act} = v_0^2/2D_r$ is an activity-induced diffusivity. Accounting for this enhancement of diffusivity, many properties of dilute ABP suspensions and their phase behavior can be explained [39,41,48,49]. The mapping, however, requires that all relevant length scales in the problem are large compared to the persistence length (or swim length) $\ell_p = v_0/D_r$ and that one probes the system on length scales larger than that [42,43,47].

The high-density dynamics of ABPs is less well explored. To describe glassy behavior of active systems, theories of the glass transition have been extended from the passive near-equilibrium case to include self-propulsion [29,46,50–55], using different models and various approximations. One particular reference point for the passive Brownian system is the mode-coupling theory of the glass transition (MCT), both in three dimensions (3D) [56,57] and in 2D [58]. Mode-coupling theory has been extended to deal with spherical ABPs in the effective-diffusion limit [51]. In this limit, the equations of motion (1) can be formally reduced to eliminate the orientation angles θ_i as explicit variables, in a procedure akin to the well-known reduction of the phase-space Langevin equation to the configuration-space Brownian dynamics. One obtains $d\vec{r}_i = \vec{F}_i/\zeta + \sqrt{2D_{\rm eff}}d\vec{W}_i$. From the fact that $\zeta \neq 1/\beta D_{\rm eff}$, Farage and Brader [51] obtained an activity-dependent prefactor in the MCT memory kernel. This MCT approach was later extended to mixtures of active and passive particles [59]. Activity enters this theory only through the Péclet number Pe. It predicts a shift of the glass transition to higher densities, in qualitative agreement with simulation results.

However, the approach to a glass transition implies transient caging of particles on a length scale $\ell_c \sim 0.1\sigma$ (where σ is a typical particle size), over increasingly long times. It is not evident that the effective-diffusion approach remains valid as the condition $\ell_c < \ell_p$ is easily violated for typical swim speeds used in simulation and experiment. This calls for a theoretical treatment that starts directly from Eq. (1), rather than from a further reduced description of the dynamics.

Besides the ABPs, another well-studied model of active glasses is that of active Ornstein-Uhlenbeck particles (AOUPs) [27–30,52,60,61]. Here particles are described by their positions and an activity vector that represents the swimming direction and evolves according to an Ornstein-Uhlenbeck process providing colored noise for the evolution of the positions. In the athermal reference case, passive Brownian motion is neglected, so particles only move due to activity. The model thus belongs to a class where activity is modeled as leading to a persistent random walk of the particles [62–64]. A theoretical treatment based on MCT was established [52] under the simplifying assumption that the particle positions evolve on a time scale larger than the time scale governing the evolution of the activity vector. This is not unlike the effective-diffusion approximation made in previous studies of high-density ABP systems. In similar spirit, a MCT for the thermal AOUP model was derived recently using a quasiequilibrium approximation [65]. These theories require as input from simulation not only the nonequilibrium static structure factors, but also information on the velocity correlations that needs to be obtained from computer simulation. (For a more recent MCT based on a separate treatment of correlation and response functions, see Ref. [55].) Predictions of the athermal AOUP MCT of Ref. [52] have been tested in computer simulation [61]. The relaxation times close to the glass transition were found to depend nonmonotonically on the persistence time of the active motion [29]. This appears to be different for ABPs, since present simulation results do not show a nonmonotonic change of relaxation times with changing $1/D_r$ [23]. Thus the connection among different models of active colloidal systems remains to be studied in more detail.

The MCT of spherical ABPs that we develop in the following treats both the positional and orientational degrees of freedom on equal footing. This avoids the reduction to a near-equilibrium or an effective-diffusion description and allows us to study the qualitative effects of self-propulsion of various persistence lengths in the high-density regime. In particular, it allows us to study the limits $D_r \to 0$ and $D_r \to \infty$ as interesting reference cases [66] that provide valuable insight into the mechanisms by which swimming modifies the caging dynamics. Our approach is based on the integration-through-transients (ITT) formalism as a formal approach to deal with the self-propulsion force as an arbitrarily strong perturbation of the passive-equilibrium dynamics. Within ITT, the only input required for MCT is the passive-equilibrium static structure factor $S(q)$, allowing us to construct [in conjunction with a suitable liquid-state theory for $S(q)$] a parameter-free (albeit approximate) theory of ABPs.

The paper is organized as follows. In Sec. II we derive the MCT for two-dimensional spherical ABPs, including rotational degrees of freedom. Section III shows numerical results for the dynamical density correlation functions close to the glass transition. Section IV is devoted to a discussion of the dependence of the glass-transition point on activity. Section V summarizes.

II. MODE-COUPLING THEORY

The statistical information of the dynamics of a system composed of N spherical ABPs is encoded in the Smoluchowski equation for the configuration-space distribution function $p(\Gamma,t)$, i.e., the probability density that corresponds to the Markov process described by the stochastic differential equations (1). Here $\Gamma = (\Gamma_r,\Gamma_\theta) = (\vec{r}_1,\ldots,\vec{r}_N,\theta_1,\ldots,\theta_N)$ labels points in configuration space. There holds $\partial_t p(\Gamma,t) = \Omega(\Gamma)p(\Gamma,t)$ with the Smoluchowski operator (in two spatial dimensions)

$$\Omega = \sum_{j=1}^{N} D_t\vec{\nabla}_j\cdot(\vec{\nabla}_j - \beta\vec{F}_j) + D_r\partial_{\theta_j}^2 - v_0\vec{\nabla}_j\cdot\vec{o}(\theta_j)$$
$$= \Omega_{\rm eq}(D_t,D_r) + \delta\Omega(v_0), \qquad (2)$$

where $\delta\Omega(v_0) = -v_0\sum_j\vec{\nabla}_j\cdot\vec{o}(\theta_j)$ is the term that represents the active motion. The interaction forces are assumed to follow from a spherically symmetric interaction potential $\vec{F}_j = -\vec{\nabla}_j U(\Gamma_r)$.

Equation (2) for v_0=0 describes the passive Brownian system. It admits the equilibrium solution $p_{\rm eq}(\Gamma_r) \propto \exp[-\beta U(\Gamma_r)]$. The ITT formalism expresses averages of observables in the nonequilibrium system through historical integrals involving transient correlation functions, i.e., correlation functions that contain the full nonequilibrium time evolution but are taken with the equilibrium distribution function. The starting point of ITT is the identity $\exp[\Omega\, t] = 1 + \int_0^t dt' \exp[\Omega\, t']\,\Omega$. Using this identity to rewrite $p(t) = \exp[\Omega\, t]p(0)$, and assuming that for $t = 0$ the system starts in equilibrium, one gets a generalized Green-Kubo formula for any observable A. For the special case of the spherical ABP system,

$$\langle A\rangle_t = \langle A\rangle_{\rm eq} - \beta v_0 \int_0^t dt' \left\langle \sum_{j=1}^N \vec{o}_j \cdot \vec{F}_j e^{\Omega^\dagger t'} A \right\rangle_{\rm eq}. \quad (3)$$

For example, the density-dependent collective swim speed of ABPs, a quantity that enters coarse-grained descriptions of the phase behavior, can be expressed in the form of Eq. (3) [67]. The desire to evaluate expressions like this prompts the development of a theory of transient correlation functions. In the following, we will drop the subscript "eq" and implicitly perform all averages over the equilibrium distribution.

The collective motion of the particles is described by the local density fluctuations $\varrho(\vec{r},\theta) = \sum_{j=1}^N \delta(\vec{r} - \vec{r}_j)\delta(\theta - \theta_j)$ and their Fourier transform

$$\delta\varrho_l(\vec{q}\,) = \sum_{j=1}^N e^{i\vec{q}\cdot\vec{r}_j} e^{il\theta_j}/\sqrt{N}, \quad (4)$$

with integer angular indices $l = -\infty,\ldots,\infty$. We assume the system to remain in a homogeneous, translationally invariant, and isotropic state. Then the equilibrium static structure factor matrix depends on the wave vector only through $q = |\vec{q}\,|$,

$$S_{ll'}(q) = \langle \delta\varrho_l^*(\vec{q}\,)\delta\varrho_{l'}(\vec{q}\,)\rangle. \quad (5)$$

Also the two-point density correlation functions are diagonal in wave-vector space under these conditions. Since the interaction potential is spherically symmetric, the matrix $\boldsymbol{S}(q)$ takes the simple form

$$S_{ll'}(q) = \delta_{ll'}(1 + \delta_{l0}(S_q - 1)), \quad (6)$$

i.e., it is the unit matrix with its (00) element replaced by S_q, the usual static structure factor of the equilibrium system of spherical particles.

The time-dependent transient density correlation functions are defined as

$$S_{ll'}(\vec{q},t) = \langle \delta\varrho_l^*(\vec{q}\,)e^{\Omega^\dagger t}\delta\varrho_{l'}(\vec{q}\,)\rangle. \quad (7)$$

Here the adjoint (or backward) Smoluchowski operator provides the temporal evolution

$$\Omega^\dagger = \sum_{j=1}^N D_t(\vec{\nabla}_j + \beta\vec{F}_j)\cdot\vec{\nabla}_j + D_r\partial_{\theta_j}^2 + v_0\vec{o}_j\cdot\vec{\nabla}_j. \quad (8)$$

We use the convention that this operator acts on everything to its right, but not on the distribution function itself. There $\boldsymbol{S}(\vec{q},0) = \boldsymbol{S}(q)$ holds. The normalized correlator is defined by $\boldsymbol{\Phi}(\vec{q},t) = \boldsymbol{S}(\vec{q},t)\cdot\boldsymbol{S}^{-1}(q)$.

The correlation functions are defined in a specific laboratory frame of reference, with respect to which particle orientations are measured. For this reason, the correlation functions depend *a priori* on the direction of the wave vector $\vec{q}$. However, simple transformation rules hold to transform the correlators to a rotated reference frame. Consider a rotation around an angle α, $\vec{r} \mapsto \vec{r}\,' = \boldsymbol{D}(\alpha)\cdot\vec{r}$ and $\theta \mapsto \theta' = \theta + \alpha$, with $\boldsymbol{D}\cdot\boldsymbol{D}^T = 1$ a rotation matrix. This changes $\delta\varrho_l(\vec{q}\,) \mapsto \delta\varrho_l(\vec{q}\,')\exp[il\alpha]$, where $\vec{q}\,' = \boldsymbol{D}\cdot\vec{q}$. The transformation is thus given by a unitary representation $\boldsymbol{u}(\alpha)$ of the orientation group SO(1), given by $u_{ll'} = \exp[-il\alpha]\delta_{ll'}$. [There holds $\boldsymbol{u}(\alpha)\cdot\boldsymbol{u}(\beta) = \boldsymbol{u}(\alpha+\beta)$, $\boldsymbol{u}(\alpha)\boldsymbol{u}^\dagger(\alpha) = \boldsymbol{1}$, $\boldsymbol{u}(0) = \boldsymbol{1}$, and $\boldsymbol{u}(\alpha + 2\pi) = \boldsymbol{u}(\alpha)$, as well as $\det\boldsymbol{u} = 1$.] One easily shows that the Smoluchowski operator itself is invariant under rotation $\Omega(\Gamma) = \Omega'(\Gamma')$, separately in all its terms. To see this, recall $\vec{\partial}\,'\cdot\vec{o}(\theta') = (\boldsymbol{D}^{-1}\cdot\vec{\partial})\cdot\vec{o}(\theta+\alpha) = \vec{\partial}\cdot\boldsymbol{D}\cdot\vec{o}(\theta+\alpha) = \vec{\partial}\cdot\vec{o}(\theta)$. Under rotation, the equilibrium distribution function remains invariant and thus one obtains the transformation rule

$$\boldsymbol{S}(\vec{q},t) \mapsto \boldsymbol{u}(\alpha)\cdot\boldsymbol{S}(\vec{q}\,',t)\cdot\boldsymbol{u}^\dagger(\alpha). \quad (9)$$

We will make use of this relation to restrict the discussion of the correlation functions to wave vectors aligned with a particular spatial direction, chosen by $\vec{q} = q\vec{e}_y$. Note that Eq. (9) confirms that $S_{00}(q,t)$ is in fact invariant under rotations.

An equation of motion for $\boldsymbol{S}(\vec{q},t)$ can be derived using the Mori-Zwanzig projection operator formalism. Observe that the equilibrium average equips the space of observables with a scalar product $\langle\delta A|\delta B\rangle \equiv \langle\delta A^*\delta B\rangle$. With this, one introduces the projection operator onto density fluctuations

$$\mathcal{P} = \sum_{l_1 l_2} \delta\varrho_{l_1}(\vec{q}\,)\rangle S^{-1}_{l_1 l_2}(q)\langle\delta\varrho^*_{l_2}(\vec{q}\,) \quad (10)$$

and sets $\mathcal{Q} = 1 - \mathcal{P}$. One now writes $\partial_t\exp[\Omega^\dagger t] = \Omega^\dagger(\mathcal{P}+\mathcal{Q})\exp[\Omega^\dagger t]$ and rewrites the second term using the Dyson decomposition

$$e^{\Omega^\dagger t} = e^{\Omega^\dagger \mathcal{Q} t} + \int_0^t dt' e^{\Omega^\dagger \mathcal{Q}(t-t')}\,\Omega^\dagger\,\mathcal{P}\,e^{\Omega^\dagger t'} \quad (11)$$

to obtain

$$\partial_t\boldsymbol{S}(\vec{q},t) = -\boldsymbol{\omega}(\vec{q}\,)\cdot\boldsymbol{S}^{-1}(q)\cdot\boldsymbol{S}(\vec{q},t) + \int_0^t dt'\boldsymbol{K}(\vec{q},t-t')\cdot\boldsymbol{S}^{-1}(q)\cdot\boldsymbol{S}(\vec{q},t'), \quad (12)$$

where $\boldsymbol{\omega}(\vec{q}\,)$ generalizes the collective diffusion matrix

$$\omega_{ll'}(\vec{q}\,) = -\langle\delta\varrho_l^*(\vec{q}\,)\,\Omega^\dagger\,\delta\varrho_{l'}(\vec{q}\,)\rangle = (q^2D_t + l^2D_r)\delta_{ll'} - \frac{iqv_0}{2}e^{-i(l-l')\vartheta_q}S_{ll}(q)\delta_{|l-l'|,1}, \quad (13)$$

writing $\vec{q} = q(\cos\vartheta_q, \sin\vartheta_q)^T$. The memory kernel $\boldsymbol{K}(\vec{q},t)$ is given by

$$K_{ll'}(\vec{q},t) = \langle\delta\varrho_l^*(\vec{q}\,)\,\Omega^\dagger\,\mathcal{Q}\,e^{\mathcal{Q}\Omega^\dagger\mathcal{Q}t}\,\mathcal{Q}\,\Omega^\dagger\,\delta\varrho_{l'}(\vec{q}\,)\rangle. \quad (14)$$

It describes the renormalization of the diffusion matrix due to many-body interactions.

For small density $\rho = N/V \to 0$ (where V is the system volume), the memory kernel in Eq. (12) vanishes. Also, the distinction between transient and stationary density correlation

functions can be dropped. The formal solution $\boldsymbol{S}(\vec{q},t) = \exp[-\boldsymbol{\omega}(\vec{q}\,)t]$ then agrees with the exact solution of the Smoluchowski equation in terms of spheroidal wave functions in 3D (which reduce to Mathieu functions in 2D) [47].

The slowing down of the dynamics close to a glass transition is driven by slow positional-density fluctuations. This suggests the splitting of the time-evolution operator $\Omega = \Omega_T(D_t, v_0) + \Omega_R(D_r)$. The matrix elements of the translational and rotational parts will be written as $\boldsymbol{\omega}(\vec{q}\,) = \boldsymbol{\omega}_T(\vec{q}\,) + \boldsymbol{\omega}_R(\vec{q}\,)$, i.e., $\omega_{R,ll'}(\vec{q}\,) = l^2 D_r \delta_{ll'}$. Correspondingly, we decompose the memory kernel into four contributions $\boldsymbol{K}(t) = \boldsymbol{K}^{TT}(t) + \boldsymbol{K}^{TR}(t) + \boldsymbol{K}^{RT}(t) + \boldsymbol{K}^{RR}(t)$, given by replacing the operators $\Omega^\dagger$ appearing to the right and to the left of the reduced propagator in Eq. (14) by their decompositions.

Since in our model of spherical ABPs the rotational degrees of freedom never slow down, all contributions to the memory kernel involving $\Omega_R^\dagger$ vanish and $\boldsymbol{K}(t) = \boldsymbol{K}^{TT}(t)$ holds. This is explicitly checked by noting that $\Omega_R^\dagger$ is self-adjoint with respect to the Boltzmann-weighted scalar product and that $\Omega_R^\dagger\, \delta\varrho_l^*(\vec{q}\,) = -D_r l^2 \delta\varrho_l^*(\vec{q}\,)$. Since $\boldsymbol{K}(t)$ evolves explicitly in the subspace orthogonal to the one-point density fluctuations, the contributions arising from $\Omega_R^\dagger$ vanish in the present case.

To describe the slow dynamics arising from a coupling of translational modes, we follow the standard procedure of MCT and rewrite the diffusion kernel $\boldsymbol{K}^{TT}(t)$ in terms of a friction kernel. To do so, we introduce a further projector

$$\mathcal{P}' = -\sum_{l_1 l_2} \delta\varrho_{l_1}(\vec{q}\,)\rangle\omega^{-1}_{T,l_1 l_2}(\vec{q}\,)\langle\delta\varrho^*_{l_2}(\vec{q}\,)\,\Omega_T^\dagger\,. \tag{15}$$

We now decompose the propagator that appears in Eq. (14) according to

$$e^{\mathcal{Q}\,\Omega_T^\dagger\,\mathcal{Q}\,t} = e^{\mathcal{Q}\,\Omega_T^\dagger\,\mathcal{Q}'\,\mathcal{Q}\,t} + \int_0^t dt' e^{\mathcal{Q}\,\Omega_T^\dagger\,\mathcal{Q}(t-t')} \times\, \mathcal{Q}\,\Omega_T^\dagger\,\mathcal{P}'\,\mathcal{Q}\,e^{\mathcal{Q}\,\Omega_T^\dagger\,\mathcal{Q}'\,\mathcal{Q}\,t'}. \tag{16}$$

This results in

$$\boldsymbol{K}^{TT}(\vec{q},t) = \boldsymbol{M}(\vec{q},t) - \int_0^t \boldsymbol{K}^{TT}(\vec{q},t-t')\cdot\boldsymbol{\omega}_T^{-1}(\vec{q}\,)\cdot\boldsymbol{M}(\vec{q},t'), \tag{17}$$

where we have defined the friction memory kernel

$$M_{ll'}(\vec{q},t) = \langle\delta\varrho_l^*(\vec{q}\,)\,\Omega_T^\dagger\,\mathcal{Q}\,e^{\mathcal{Q}\,\Omega_T^\dagger\,\mathcal{Q}'\,\mathcal{Q}\,t}\,\mathcal{Q}\,\Omega_T^\dagger\,\delta\varrho_{l'}(\vec{q}\,)\rangle. \tag{18}$$

Note that $\boldsymbol{M}(\vec{q},t)$ and $\boldsymbol{K}^{TT}(\vec{q},t)$ only differ in their time evolution. In the context of passive Brownian particles, the operator appearing in the exponential of Eq. (18) is also referred to as the one-particle irreducible Smoluchowski operator [68].

Equations (12) and (17) can be combined to a time-evolution equation for the density correlation functions that is a suitable starting point for approximations of the slow dynamics arising from the slow evolution of positional-density fluctuations,

$$\boldsymbol{\omega}_T^{-1}(\vec{q}\,)\cdot\partial_t\boldsymbol{S}(\vec{q},t) + [\boldsymbol{S}^{-1}(q) + \boldsymbol{\omega}_T^{-1}(\vec{q}\,)\cdot\boldsymbol{\omega}_R]\cdot\boldsymbol{S}(\vec{q},t) + \int_0^t dt'\boldsymbol{m}(\vec{q},t-t')\cdot[\partial_{t'}\boldsymbol{S}(\vec{q},t') + \boldsymbol{\omega}_R\cdot\boldsymbol{S}(\vec{q},t')] = \boldsymbol{0}. \tag{19a}$$

Here we have used that $\boldsymbol{\omega}_R\cdot\boldsymbol{S}^{-1}(q) = \boldsymbol{\omega}_R$ for the spherical ABP system we consider and abbreviated

$$\boldsymbol{m}(\vec{q},t) = \boldsymbol{\omega}_T^{-1}(\vec{q}\,)\cdot\boldsymbol{M}(\vec{q},t)\cdot\boldsymbol{\omega}_T^{-1}(\vec{q}\,). \tag{19b}$$

Equations (19) are the starting point of mode-coupling approximations for glassy dynamics. Setting $v_0 = 0$, the matrices all become diagonal (since $\Omega_T^\dagger$ does not mix translational and rotational degrees of freedom in this case) and one recovers for $S_{00}(q,t)$ the standard Mori-Zwanzig equation used to derive MCT for Brownian spherical particles.

Rotational diffusion appears in Eqs. (19) in the form of a hopping term in the MCT language, viz., the last term under the integral in Eq. (19a). This term causes a considerable complication in the analysis of the MCT equation of motion, but it has a clear physical significance: By construction of the spherical ABP model, rotation remains unhindered even in the dense system and even in the glass and therefore the associated density fluctuations for $l \neq 0$ need to decay (exponentially) on a time scale $1/l^2 D_r$. The last term in Eq. (19a) ensures this.

The original MCT only contains a convolution of the memory kernel with the time derivative of the density correlation function, viz., the first term under the integral in Eq. (19a). In this form the equations allow for an ideal glass transition: There exist solutions with a nonzero long-time limit $\lim_{t\to\infty}\boldsymbol{S}(\vec{q},t) = \boldsymbol{F}(\vec{q}\,) \neq \boldsymbol{0}$. Note that, despite the hopping term, Eq. (19) still allows for an ideal glass transition for all transient density correlation functions $S_{ll'}(\vec{q},t)$ with $l = 0$. This is a feature that is qualitatively different from previous MCT treatments (even of driven systems), where either no hopping term is present or the (phenomenological) inclusion of hopping causes all correlators to decay. It is a feature of standard MCT that all density-relaxation modes are strongly coupled and governed by the same scaling relations asymptotically. In the present theory, this coupling is broken with regard to the indices l by the appearance of a singular hopping matrix $\boldsymbol{\omega}_R$.

The MCT approximation now consists of two intertwined steps. First the fluctuating forces $\mathcal{Q}\,\Omega_T^\dagger\,\delta\varrho_l(\vec{q}\,)$ that appear in $\boldsymbol{M}(\vec{q},t)$ are replaced by their overlap with density-fluctuation pairs. Using the shorthand notation $\delta\varrho_1 \equiv \delta\varrho_{l_1}(\vec{q}_1)$, one introduces the pair-density projector

$$\mathcal{P}_2 = \sum_{1,2,1',2'} \delta\varrho_1\delta\varrho_2\rangle\chi_{121'2'}\langle\delta\varrho^*_{1'}\delta\varrho^*_{2'} \tag{20}$$

with a suitable normalization matrix χ. Second, the resulting dynamical four-point correlation functions that involve the reduced dynamics are replaced by the product of two-point correlation functions propagated by the full dynamics,

$$\langle\delta\varrho_1^*\delta\varrho_2^* e^{\mathcal{Q}\,\Omega_T^\dagger\,\mathcal{Q}'\,\mathcal{Q}\,t}\delta\varrho_{1'}\delta\varrho_{2'}\rangle \approx \langle\delta\varrho_1^* e^{\Omega^\dagger t}\delta\varrho_{1'}\rangle\langle\delta\varrho_2^* e^{\Omega^\dagger t}\delta\varrho_{2'}\rangle + \{1'\leftrightarrow 2'\} \tag{21}$$

together with a consistent approximation of χ. For a detailed derivation of the MCT expression for the memory kernel, we refer to Appendix A. One gets

$$m_{ll'}(\vec{q},t) \approx \frac{\rho}{2}\int\frac{d^2k}{(2\pi)^2}\sum_{l_1 l_2 l_1' l_2'}\mathcal{V}^\dagger_{ll_1l_2}(\vec{q},\vec{k},\vec{p}\,) \times S_{l_1l_1'}(\vec{k},t)S_{l_2l_2'}(\vec{p},t)\mathcal{V}_{l'l_1'l_2'}(\vec{q},\vec{k},\vec{p}\,), \tag{22}$$

with coupling coefficients (vertices) $\mathcal{V}^\dagger_{ll_1l_2}(\vec{q},\vec{k},\vec{p}\,) = \sum_m [\boldsymbol{\omega}_T^{-1}(\vec{q}\,)]_{lm}\mathcal{W}^\dagger_{ml_1l_2}(\vec{q},\vec{k},\vec{p}\,)$ and $\mathcal{V}_{ll_1l_2}(\vec{q},\vec{k},\vec{p}\,) = \sum_m (\boldsymbol{\omega}_T^{-1})_{lm}(\vec{q}\,)\mathcal{W}_{ml_1l_2}(\vec{q},\vec{k},\vec{p}\,)$. These are given in terms of the equilibrium static structure, viz.,

$$\begin{aligned}\mathcal{W}^\dagger_{ll_1l_2}(\vec{q},\vec{k},\vec{p}\,) &= D_t\delta_{l,l_1+l_2}(\vec{q}\cdot\vec{k}c_{l_1l_1}(k) + \vec{q}\cdot\vec{p}c_{l_2l_2}(p)) \\ &\quad + \frac{iv_0}{2\rho}\delta_{|l-l_1-l_2|,1}S_{l_1l_1}(q)[ke^{-i(l-l_1-l_2)\vartheta_k} \\ &\quad \times \tilde{S}_{l_1,l-l_2}(k) + pe^{-i(l-l_1-l_2)\vartheta_p}\tilde{S}_{l_2,l-l_1}(p) \\ &\quad - qe^{-i(l-l_1-l_2)\vartheta_q}],\end{aligned} \tag{23}$$

where we have defined $\tilde{S}_{ll'}(k) = S^{-1}_{ll}(k)S_{l'l'}(k)$. Here $c_{00}(q)$ is the direct correlation function defined by $S(q) = 1/[1-\rho c(q)]$ and all other elements of $c_{ll'}(q)$ vanish. The vertex $\mathcal{W}$ is the same as in equilibrium,

$$\mathcal{W}_{ll_1l_2}(\vec{q},\vec{k},\vec{p}\,) = D_t\delta_{l,l_1+l_2}(\vec{q}\cdot\vec{k}c_{l_1l_1}(k) + \vec{q}\cdot\vec{p}c_{l_2l_2}(p)). \tag{24}$$

It differs from $\mathcal{W}^\dagger$ because the time-evolution operator $\Omega^\dagger$ is not self-adjoint with respect to the scalar product defined by the equilibrium averages.

For $v_0 = 0$, these equations reduce to the equilibrium MCT expressions. In particular, in this case $\mathcal{V} = \mathcal{V}^\dagger$ no longer explicitly depends on D_t. In the active case $v_0 \neq 0$ one readily checks that the explicit dependence on D_t still cancels in the memory kernel if the self-propulsion velocity is expressed in terms of a Péclet number $\mathrm{Pe}_t = v_0\sigma/D_t$, where σ is a typical particle diameter. There is no dependence on D_r in the memory kernel and therefore the Péclet number $\mathrm{Pe} = v_0^2/D_tD_r$ does not assume the natural role in determining the MCT dynamics that it has for the low-density system.

The MCT approximation preserves the transformation properties of the correlation functions under rotation (9). In fact, the same transformation law is required for all the quantities that appear in the Mori-Zwanzig equation (12) or (19a). In particular, $\boldsymbol{\omega}(\vec{q}\,) \mapsto \boldsymbol{u}(\alpha)\cdot\boldsymbol{\omega}(\vec{q}\,')\cdot\boldsymbol{u}^\dagger(\alpha)$ is easily checked. For the MCT vertices, a straightforward calculation shows $\mathcal{W}^\dagger_{ll_1l_2}(\vec{q},\vec{k},\vec{p}\,) \mapsto \mathcal{W}^\dagger_{l'l'_1l'_2}(\vec{q}\,',\vec{k}\,',\vec{p}\,')u_{ll'}(\alpha)u^\dagger_{l'_1l_1}(\alpha)u^\dagger_{l'_2l_2}(\alpha)$ and equivalently for $\mathcal{W}_{ll_1l_2}(\vec{q},\vec{k},\vec{p}\,)$, i.e., all terms that appear in the MCT expression for $\boldsymbol{m}(\vec{q},t)$ transform like tensors.

The fact that the MCT approximation preserves the transformation properties of the correlation functions under rotation allows us to pick a coordinate system where $\vec{q}$ is aligned along a coordinate axis, say, $\vec{q} = q\vec{e}_y$. By using the unitary transformation property, all correlation functions entering the MCT memory kernel can be rewritten in terms of those evaluated with $\vec{q}$ aligned along the same axis. This allows to reduce the numerical calculation to wave vectors along a single spatial axis.

The MCT equations have been solved numerically on a grid of 128 wave numbers equally spaced up to $|\vec{q}\,| \leqslant Q$ with $Q\sigma = 50$. For numerical stability, the first five grid points are dropped in the calculation of the memory kernel. In angular indices, we use a cutoff $|l| \leqslant L$, with $L = 1$. Some results have been checked with $L = 2$ and the effects on $\Phi_{00}(\vec{q},t)$ were minor. The presence of the hopping term with its singular structure (imposed by $\omega_{R,00} = 0$) poses a numerical problem at long times. We have developed an extension of the standard algorithm that is usually employed to solve MCT equations, which we outline in Appendix B.

To determine the MCT vertex, the equilibrium static structure factor is needed. In odd dimensions, the Percus-Yevick approximation provides a reasonably accurate analytical expression. However, in even dimensions, no such analytical solution is known. We use the Baus-Colot expression for $S(q)$ that is known to be close to simulation data [69].

We fix units of length and time by the particle diameter $\sigma = 1$ and the translational free-diffusion time $\sigma^2/D_t = 1$. Densities are reported as packing fractions $\phi = (\pi/4)\rho\sigma^2$. With the chosen parameters, we obtain a glass transition in the passive hard-disk system at a critical packing fraction $\phi^c \approx 0.7208(1)$. This is slightly different from the value $\phi^c \approx 0.697$ that was reported from earlier MCT calculations [58]. In comparison to this work, we have improved the numerical evaluation of the wave-vector integrals appearing in the MCT memory kernel; see Appendix B for details.

III. DYNAMICS

Exemplary MCT results for the density correlation functions $\Phi_{00}(\vec{q},t)$ are shown in Fig. 1. A wave number $q\sigma = 8$

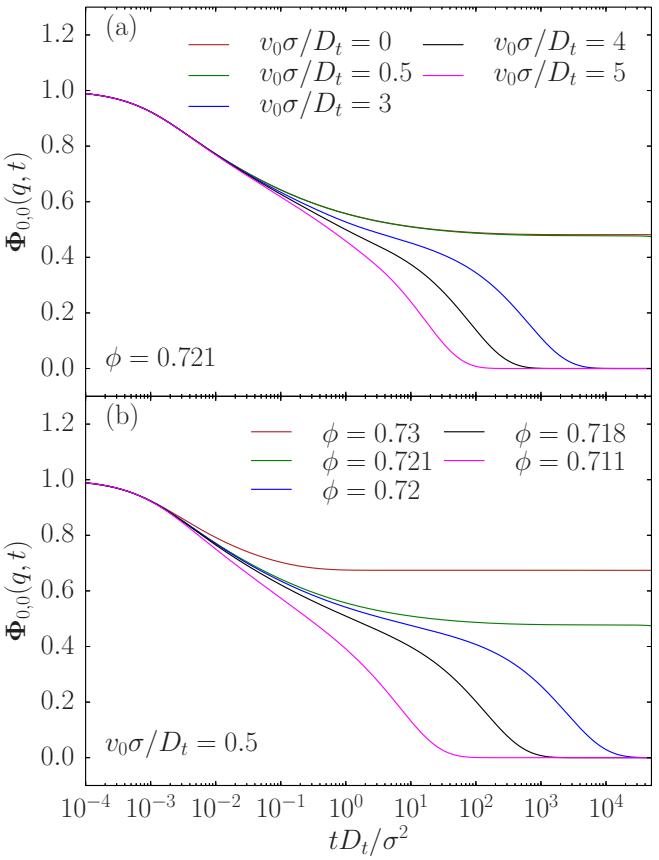

FIG. 1. Transient density correlation functions $\Phi_{00}(q,t)$ of a hard-disk ABP system within MCT, at wave number $q\sigma = 8$ and for $D_r = 1$: (a) functions at constant packing fraction $\phi = 0.721$ above the passive glass transition, for increasing v_0 (right to left) as labeled, and (b) functions at constant self-propulsion velocity v_0, for increasing packing fraction (left to right).

in the vicinity of the main peak of the equilibrium $S(q)$ was chosen. The density correlation functions show the qualitative features expected for dense colloidal suspensions nearing dynamical arrest: After an initial relaxation, a plateau emerges at high densities that extends over an increasingly large intermediate-time window as the density is increased. The final relaxation from this plateau to zero is termed structural relaxation and its characteristic time increases strongly with increasing density. At the highest densities shown, structural relaxation becomes ineffective and is not seen over the full time window accessible to the numerical solution scheme. Hence, $\lim_{t\to\infty} S_{00}(\vec{q},t) = F_{00}(\vec{q}\,) > 0$. This nonzero positive nonergodicity parameter signals the appearance of an ideal glass.

With increasing self-propulsion velocity v_0, the dynamics speeds up, as shown in Fig. 1(a). Self-propulsion renders the particle motion more vivid and this opposes the slow dynamics. This result is also qualitatively consistent with earlier Brownian-dynamics (BD) simulation studies of three-dimensional ABPs [23]. (Note that, there, stationary-state nonequilibrium correlation functions were reported, while the central objects of our MCT are the transient nonequilibrium, equilibrium-averaged correlation functions.)

For small enough self-propulsion velocity, the glass remains stable at sufficiently high density. This is exemplified by Fig. 1(b), where curves for constant $v_0 = 0.5 D_t/\sigma$ are shown. At the highest packing fractions shown, no sign of structural relaxation can be seen in the numerical results over the time window covered in the figure.

Hence, for small enough but finite v_0 MCT predicts an ideal active glass. As Fig. 1(b) demonstrates, the signature of the transition to this active glass is qualitatively as for the passive ideal glass: With increasing density at fixed v_0, structural relaxation dramatically slows down until it completely arrests at the transition density ϕ^c. Further increasing the density causes the nonergodicity parameter to increase. The ideal glass transition is discontinuous in the sense that the long-time limit of the density correlation functions jumps from zero in the liquid ($\phi < \phi^c$) to a finite value at ϕ^c.

These results suggest that there is a line of ideal glass transitions (ϕ^c, v_0^c) in the density–self-propulsion plane. This line shifts to increasing density with increasing v_0. Qualitatively, this result was derived in earlier extensions of MCT that do not account for orientational degrees of freedom explicitly [51].

With the present approach, the influence of the rotational diffusion coefficient on the dynamics can be studied. Figure 2 exemplifies the effects of increasing D_r on the dynamics at fixed self-propulsion velocity. Keeping the other parameters fixed, an increase in D_r leads to a slowing down of the structural-relaxation dynamics. Qualitatively, this is expected from the argument that faster reorientation of the individual particles causes the self-propulsion to be less effective in melting nearest-neighbor cages, since for the latter process a certain persistence of the self-propulsion force in a specific direction needs to be maintained. In other words, a decrease in persistence time $1/D_r$ causes the system to be less active in the regime of structural relaxation. The slowing down with increasing D_r (i.e., decreasing persistence time) is more pronounced at higher densities: While at $\phi = 0.7$ the final relaxation of the curves shown in Fig. 2 spreads out by about a

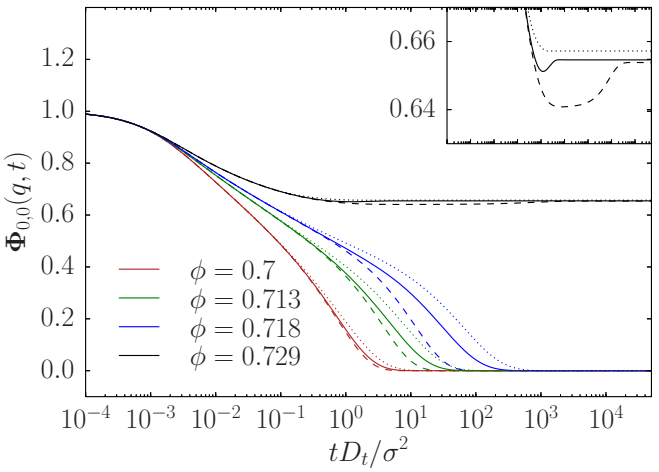

FIG. 2. Density correlation functions $\Phi_{00}(\vec{q},t)$ for packing fractions $\phi = 0.7$, 0.713, 0.718, and 0.729 (groups of lines from left to right) for $q\sigma = 8$ and self-propulsion velocity $v_0 = 3D_t/\sigma$ for different values of the rotational diffusion coefficient $D_r = 1/1000$, 1, and 10 (dashed, solid, and dotted lines). The inset provides a close-up of the $\phi = 0.729$ curves.

factor 2, the same change in D_r causes the structural-relaxation time to change by a factor of about 10 at $\phi = 0.718$.

The structural relaxation dynamics of the weakly active system shows the same qualitative features as they are known from the passive system. In particular, the structural relaxation process can be well described by a stretched-exponential function in time for the cases shown in Figs. 1 and 2. It is known from the passive system that density fluctuations with wavelengths comparable to the particle size govern the slow dynamics.

For the active system, the persistence of self-propulsion sets another length scale $\ell_p = v_0/D_r$. This suggests that we should discuss the effect of density fluctuations on length scales much larger than, comparable to, and much smaller than the persistence length. Let us introduce a rescaled wave number $\tilde{q} = q\ell_p/2\pi$. The low-density dynamics of ABPs exhibits three distinct regimes [47]. For $\tilde{q} \ll 1$, one probes the dynamics on length scales large compared to ℓ_p and hence one sees diffusive relaxation with a diffusion coefficient $D_{\rm eff}(\mathrm{Pe})$. For small length scales, probed by $\tilde{q} \gg 1$, the initial Brownian passive diffusion of the ABP is seen and the density correlators decay diffusively, with diffusion coefficient D_t. Activity causes an intermediate regime $\tilde{q} \approx 1$ to appear, where the persistent swimming motion affects the relaxation of density fluctuations. Over the length scales probed in this regime, particles swim in a fixed direction and cause density fluctuations to decay in a damped-oscillatory fashion, leading to pronounced undershoots in the final relaxation.

The influence of high-density interactions on this single-particle picture is examined in Fig. 3. Here state points close to the glass transition were chosen and to make a connection to the low-density theory, different activities along a cut with constant Péclet number $\mathrm{Pe} = 32$ are shown. Figures 3(a)–3(f) correspond to increasing self-propulsion velocity [from Figs. 3(a) to 3(f)] and at fixed Pe, these correspond to decreasing persistence lengths. Essentially, the low-density

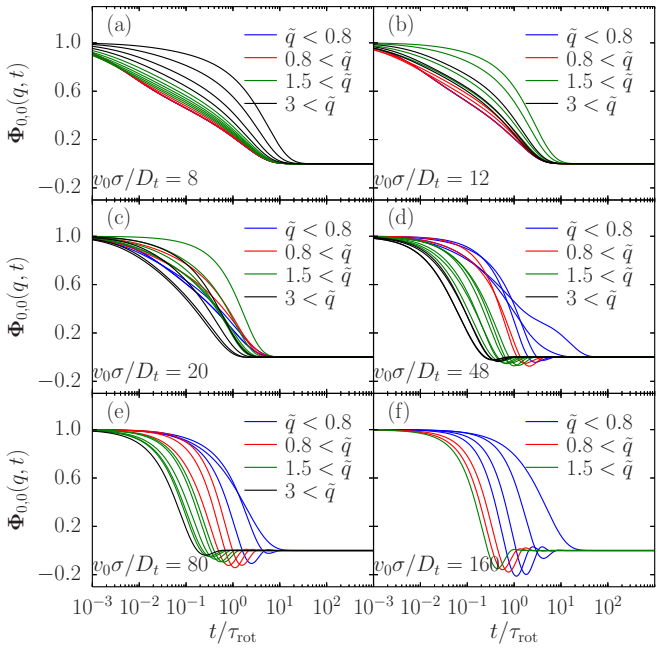

FIG. 3. Wave-number dependence of the transient density correlation functions $\Phi_{00}(q,t)$ for packing fraction $\phi = 0.719$ just below the passive glass transition and different velocities as labeled, keeping the Péclet number $\mathrm{Pe} = v_0^2/D_r D_t = 32$ fixed. The values are (a) $(v_0, D_r) = (8,2)$, (b) $(v_0, D_r) = (12,4.5)$, (c) $(v_0, D_r) = (20,12.5)$, (d) $(v_0, D_r) = (48,64)$, (e) $(v_0, D_r) = (80,200)$, and (f) $(v_0, D_r) = (160,800)$. Wave numbers $\tilde{q} = q\ell_p/2\pi$ are given in units of the persistence length $\ell_p = v_0/D_r$ and increase from right to left (in the top part of the curves): (a) $\ell_p = 4$, (b) $\ell_p = 2.67$, (c) $\ell_p = 1.6$, (d) $\ell_p = 0.75$, (e) $\ell_p = 0.4$, and (f) $\ell_p = 0.2$. Correlators are shown as functions of rescaled time $t/\tau_{\rm rot}$ with the time scale set by the orientational diffusion $\tau_r = 1/D_r$.

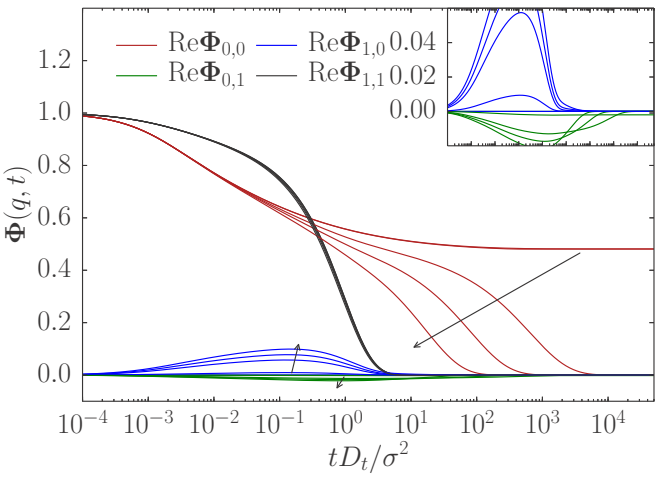

FIG. 4. Matrix elements of the transient density correlation matrix $\mathbf{\Phi}(\vec{q},t)$ at fixed packing fraction $\phi = 0.721$ and rotational diffusion $D_r = 1D_t/\sigma^2$ for increasing v_0 (as indicated by arrows). The inset provides a close-up of the off-diagonal components.

scenario is recovered for the case $\ell_p < \sigma$, i.e., for large self-propulsion velocity. There structural arrest is effectively destroyed by active driving and the correlation functions decay on a time scale $\tau_{\rm rot} = 1/D_r$, showing oscillations around $\tilde{q} \approx 1$ [cf. Figs. 3(e) and 3(f)].

For large persistence length $\ell_p \gg \sigma$, Figs. 3(a) and 3(b) demonstrate that the low-density scenario is absent. Here all correlation functions decay without oscillations. This result can be interpreted as showing that once the interparticle length scale becomes smaller than ℓ_p, density fluctuations can no longer be translated by persistent motion; they relax by the combination of diffusion and activity-modified structural interactions. Coincidentally, for the $\ell_p \gg \sigma$ cases shown in Fig. 3, the intermediate-time plateau of structural relaxation begins to emerge at large $\tilde{q}$ (corresponding to intermediate $q\sigma$).

The appearance of oscillatory relaxation in the density correlation functions of a Brownian system is a clear signature of nonequilibrium dynamics. Recall that the equilibrium Smoluchowski operator $\Omega_{\rm eq}$ is negative semidefinite, i.e., it has nonpositive real eigenvalues only. As a result, the equilibrium autocorrelation functions are completely monotonic functions: They can be written as superpositions of purely relaxing exponential functions with positive weights. This is a feature that is preserved under the MCT approximation [70,71]. The ITT approach we employ here allows us to account for the change in the spectral properties of Ω that are induced by active motion and are not captured by the effective-diffusion approximations of earlier theories [51,65]. Note that similar nonequilibrium signatures were seen in the relaxation patterns of sufficiently strongly sheared systems [72] and of a driven probe particle in a passive suspension [73].

To highlight the dynamics of the reorientational degrees of freedom, we show in Fig. 4 the matrix elements of $\Phi_{ll'}(\vec{q},t)$ for $|l| \leqslant 1$. Only positive l and l' are shown for simplicity and the case $l = l' = 0$ is repeated from above for reference. The $(ll') = (11)$ correlator reflects the decay of orientational order. It decays on the time scale $\tau_{\rm rot} = 1/D_r$, with a final exponential relaxation. This is expected since in the spherical ABP model, rotation is not influenced by the packing of particles. Note that the decay of $\Phi_{11}(\vec{q},t)$ is not that of a single exponential; even at low densities and without self-propulsion, $\Phi_{11}(\vec{q},t) \sim \exp[-q^2 D_t t]\exp[-D_r t]$. In general, the $(ll') = (11)$ correlator inherits a signature of the translational motion for $t \ll \tau_{\rm rot}$, which is cut off by an exponential decay at $t \sim \tau_{\rm rot}$.

The off-diagonal elements $(ll') = (01)$ and (10) of the transient density correlation function behave differently from each other. In equilibrium, the matrix of correlation functions needs to be symmetric (as is the case, for example, in the MCT developed for Newtonian nonspherical particles [74–77]). This symmetry is lost in the present theory for the transient (nonstationary) correlation functions because the time-evolution operator is not self-adjoint with respect to the equilibrium-weighted scalar product.

The off-diagonal elements vanish with $v_0 \to 0$, as expected from the structure of the Smoluchowski equation for spherical ABPs. Interestingly, the correlation function $\Phi_{01}(\vec{q},t)$ shows nontrivial slow dynamics that is coupled to the slow dynamics of the positional-density correlator $\Phi_{00}(\vec{q},t)$. In particular, it displays structural relaxation that slows down beyond the time scale τ_r over which orientational order decays. The correlation function $\Phi_{10}(\vec{q},t)$ instead decays on the reorientational time scale $\tau_{\rm rot}$.

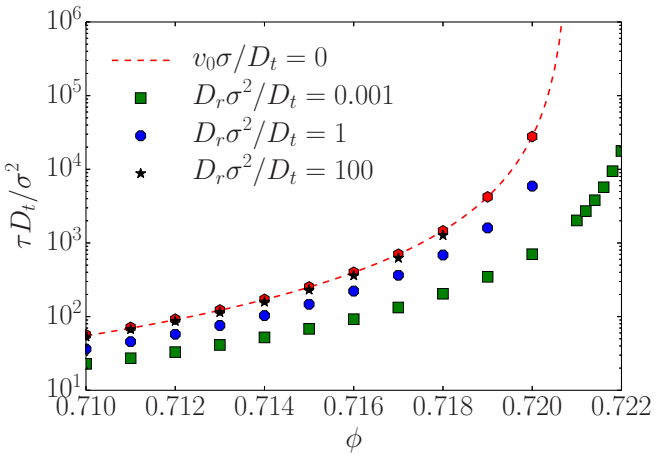

FIG. 5. Structural relaxation times $\tau(\phi, v_0, D_r)$ as a function of packing fraction ϕ for fixed $v_0 = 2D_t/\sigma$ and different D_r (as labeled by the different symbols). Hexagons connected by a dashed line correspond to the passive system.

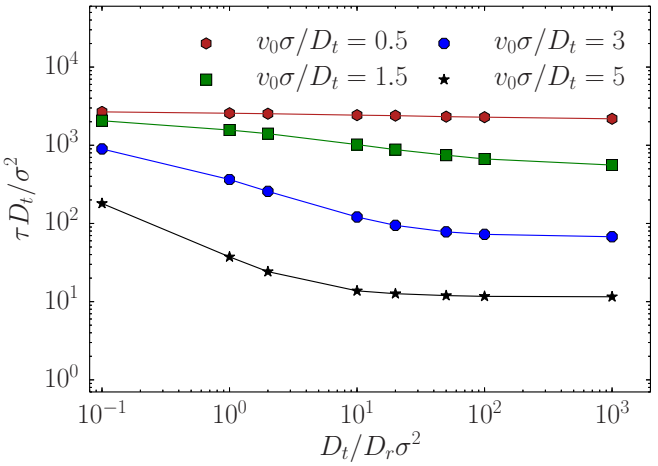

FIG. 6. Structural relaxation times τ as a function of the persistence time $1/D_r$ for fixed self-propulsion velocities v_0 (different symbols as labeled) at packing fraction $\phi = 0.719$.

This observation can be rationalized by the peculiar structure of the equations of motion of spherical ABPs: Orientations influence the slow dynamics of the positions, but not vice versa. Thus, the evolution of positional-density fluctuations $|\exp[\Omega^\dagger t]\delta\varrho_0(\vec{q}\,)\rangle$ will not be detectable in the subspace spanned by the orientations $\langle\delta\varrho_1(\vec{q}\,)|$ for times $t \gg \tau_{\rm rot}$. On the other hand, the impact of the time-evolved initial polar order $|\exp[\Omega^\dagger t]\delta\varrho_1(\vec{q}\,)\rangle$ on the positional-density fluctuations of the system $\langle\delta\varrho_0(\vec{q}\,)|$ persists until the time of overall structural relaxation, hence $S_{01}(\vec{q},t) = \langle\delta\varrho_0(\vec{q}\,)|\exp[\Omega^\dagger t]\delta\varrho_1(\vec{q}\,)\rangle$ decays as slow as $S_{00}(\vec{q},t)$.

The usual quantification of the slow dynamics is in terms of the structural relaxation time τ. Following the operational definition used in many studies of glassy dynamics, we define τ as the time where the density-correlation function has decayed to 1% of its initial value $\Phi_{00}(\vec{q},\tau) = 0.01$.

Results for $\tau(\phi)$ for a fixed self-propulsion velocity are shown in Fig. 5. As anticipated from the discussion above, the structural relaxation time strongly increases with increasing packing fraction, in a power-law fashion that is the hallmark of the approach to the MCT glass transition. At fixed v_0, increasing D_r increases the structural relaxation time. For $D_r \to \infty$, the τ-vs-ϕ curve corresponding to the passive system is approached.

The data shown in Fig. 5 agree qualitatively with corresponding three-dimensional results from BD simulations [23]. Again, similar results have been discussed for the AOUP system [61] and glassy tissue models [6], although some features of the dynamics may be quite different from those in ABPs. This is not unexpected, because the fact that structural relaxation times slow down as a power law upon approaching an MCT glass transition is deeply rooted in the structure of the theory and thus is a very robust prediction. In particular, also the approach to the glass transition at fixed packing fraction but decreasing v_0 yields a power-law increase in the structural relaxation time.

The influence of the persistence time $1/D_r$ on the structural relaxation is further elucidated by discussing $\tau(1/D_r)$ at fixed self-propulsion velocity. The MCT results are shown in Fig. 6 and can be readily compared with results for the AOUP model of Ref. [29]. There a nonmonotonic behavior was observed, i.e., the relaxation time τ first decreased with increasing $1/D_r$ and then increased with further increasing $1/D_r$. For the ABP model, we obtain only an initial decrease of τ with increasing $1/D_r$, from the value corresponding to the passive system to a smaller value that becomes independent of D_r in the limit $1/D_r \to \infty$. That the initial decrease is seen similarly in both models is due to the fact that in both cases, passive Brownian motion is approached for $1/D_r \to 0$. Note, however, that in the AOUP model (which does not include thermal diffusion), the activity itself generates this Brownian motion, while in the case of ABPs, activity becomes ineffective compared to the translational diffusivity. One can rationalize the different behavior at large $1/D_r$ in a similar vein: Recall that in the AOUP model, activity is the sole driving force beyond particle interactions and thus the infinitely persistent motion is quite different from the one encountered in the ABPs. Thus, infinitely persistent AOUPs can block themselves (inhibiting structural relaxation), while a finite translational diffusion coefficient D_t in ABPs will cause such blocking to be ineffective.

The structural relaxation time depends on the wave number of the density fluctuations. The q dependence of τ is shown for a fixed density and various self-propulsion velocities in Fig. 7. Both of the slow relaxation times for $(ll') = (00)$ and (01) are shown. Here the definition $\Phi_{0l'}(\vec{q},\tau) = 10^{-6}$ has been used to account for the small magnitude of $\Phi_{01}(\vec{q},t)$. From the passive case, it is known that $\tau(q)$ is an oscillating decaying function of q, with oscillations in phase with those of the equilibrium static structure factor $S(q)$. This typical signature of glassy dynamics is visible in Fig. 7 also for the active system. Increasing self-propulsion velocity shifts the relaxation times to shorter values, essentially by the same amount for all q for the range of v_0 shown. This emphasizes that the active enhancement of structural relaxation in this case is a collective effect. Note that here $\ell_p > \sigma$, i.e., the results are for the regime in Fig. 3 where density fluctuations cannot be shifted by persistent motion.

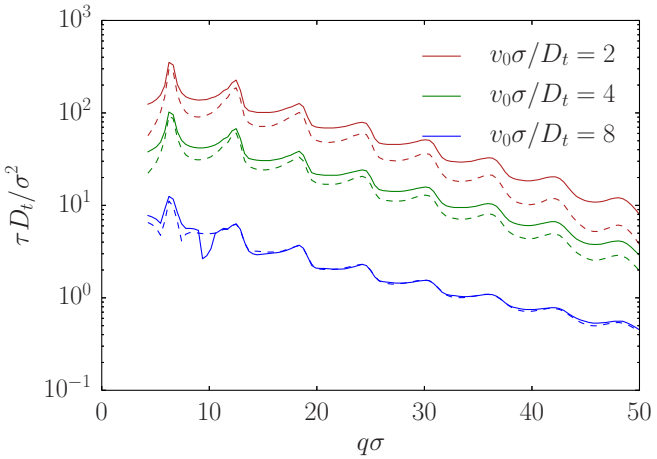

FIG. 7. Structural relaxation times $\tau(\phi, v_0, D_r)$ as a function of wave number q for fixed $D_r = 1 D_t/\sigma^2$ and various v_0 as indicated (increasing v_0 from top to bottom). Solid lines are extracted from the positional-density correlator $\Phi_{00}(\vec{q},t)$ and dashed lines from the orientational correlator $\Phi_{01}(\vec{q},t)$.

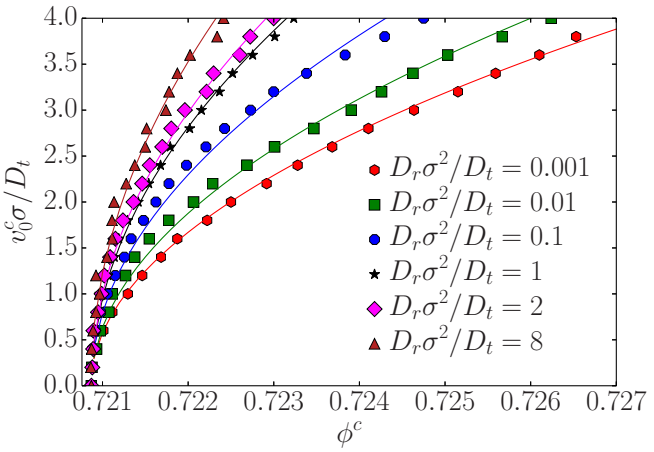

FIG. 8. Active-glass-transition lines obtained from power-law fits to the structural relaxation times $\tau(\phi)$ obtained from the transient density correlators $\Phi_{00}(\vec{q},t)$. Symbols correspond to different choices for D_r as labeled (increasing from bottom to top). Lines are fits with $v_0^c = A(D_r)\sqrt{\phi^c - \phi_0^c}$, where ϕ_0^c is the glass-transition point of the passive system.

The relaxation times of the $(ll') = (01)$ correlator (dashed lines in Fig. 7) show the same qualitative behavior as those of the $(ll') = (00)$ correlator. Approaching the glass transition, all slow relaxation modes that are relevant within MCT become strongly coupled, so one expects the approach to a common scaling behavior. This can indeed be seen for $v_0 = 4D_t/\sigma$ and $v_0 = 2D_t/\sigma$ in the figure. For the larger $v_0 = 8D_t/\sigma$, the τ-versus-q curves corresponding to the two correlators ($l' = 0$ and $l' = 1$) become identical at large q. At the same time, the oscillations in q become slightly less pronounced. This indicates that the dynamics on short length scales and for strong self-propulsion loses its collective character and becomes more incoherent.

IV. GLASS TRANSITION

The ideal glass transition is signaled by the appearance of a nonzero nonergodicity parameter $\boldsymbol{F}(\vec{q}\,) = \lim_{t\to\infty} \boldsymbol{S}(\vec{q},t) \neq \boldsymbol{0}$. In the standard MCT, one derives a separate algebraic equation for $\boldsymbol{F}(\vec{q}\,)$ from the long-time behavior of the equations of motion. This assumes that the solutions $\boldsymbol{S}(\vec{q},t)$ are slowly varying functions such that the time derivatives of the correlation functions become arbitrarily small at long times. The same procedure applies here in the case $D_r = 0$, where $\boldsymbol{\omega}_R = \boldsymbol{0}$. Then one arrives at

$$\boldsymbol{F}(\vec{q}\,) + \boldsymbol{m}(\vec{q}\,) \cdot [\boldsymbol{F}(\vec{q}\,) - \boldsymbol{S}(q)] = \boldsymbol{0}, \tag{25}$$

where we use the shorthand $\boldsymbol{m}(\vec{q}\,) \equiv \lim_{t\to\infty} \boldsymbol{m}(\vec{q},t)$. Equation (25) is a nonlinear implicit equation for $\boldsymbol{F}(\vec{q}\,)$, since $\boldsymbol{m}(\vec{q}\,)$ is a bilinear functional of these matrices. Generically, there appear bifurcation points where the physically relevant solution of Eq. (25) changes from the liquidlike $\boldsymbol{F}(\vec{q}\,) = \boldsymbol{0}$ to some glasslike $\boldsymbol{F}(\vec{q}\,) \neq \boldsymbol{0}$. These bifurcations indicate idealized glass-transition points [56]. Note that Eq. (25) is an algebraic equation that can be evaluated without solving the time-dependent MCT equations.

The presence of the term $\boldsymbol{\omega}_R \neq \boldsymbol{0}$ complicates the determination of the $t \to \infty$ limit of $\boldsymbol{S}(\vec{q},t)$. From a Laplace transform of Eq. (19), one finds that the long-time limits need to obey

$$\boldsymbol{m}(\vec{q}\,) \cdot \boldsymbol{\omega}_R \cdot \boldsymbol{F}(\vec{q}\,) = \boldsymbol{0}, \tag{26a}$$

together with

$$\boldsymbol{F}(\vec{q}\,) + \boldsymbol{m}(\vec{q}\,) \cdot [\boldsymbol{F}(\vec{q}\,) - \boldsymbol{S}(q) + \boldsymbol{\omega}_R \boldsymbol{S}_0(\vec{q}\,)] = \boldsymbol{0}, \tag{26b}$$

where $\boldsymbol{\omega}_R \boldsymbol{S}_0(\vec{q}\,) \equiv \int_0^\infty dt\, \boldsymbol{\omega}_R \cdot \boldsymbol{S}(\vec{q},t)$ is the integral over the decaying matrix elements of the correlator. Here we have assumed that the ultimate relaxation to the long-time value is faster than algebraic, motivated by the presence of exponentially decaying $l \neq 0$ modes. Unlike Eq. (25), Eq. (26b) is no longer an equation that involves only the long-time limits of the correlators and their memory kernels; through $\boldsymbol{\omega}_R \boldsymbol{S}_0(\vec{q}\,)$, details on the full time evolution enter. Still, bifurcation points in Eq. (26b) should signal idealized glass transitions, and the asymptotic analysis of the MCT equations close to these transition points proceeds in analogy to the passive case [56]. However, with our current algorithm we found the numerical evaluation of the bifurcation points of Eq. (26b) to be too unstable, because they depend sensitively on a precise evaluation of $\boldsymbol{\omega}_R \boldsymbol{S}_0(\vec{q}\,)$.

We have therefore determined tentative glass-transition points from extrapolations of the τ-vs-ϕ curves using the expected asymptotic MCT power laws $\tau \sim |\phi - \phi^c|^{-\gamma}$. All three parameters (amplitude, exponent, and critical point) in this asymptotic formula were allowed to depend on the model parameters v_0 and D_r. The results for various fixed D_r are shown in Fig. 8 as glass-transition lines in the (ϕ, v_0) plane. The transition lines depend on both v_0 and D_r explicitly and we did not observe a collapse of the curves when either Pe or ℓ_p was kept fixed.

Qualitatively, these extrapolations confirm the observations made above: Increasing self-propulsion speed shifts the glass transition to higher densities and increasing the rotational

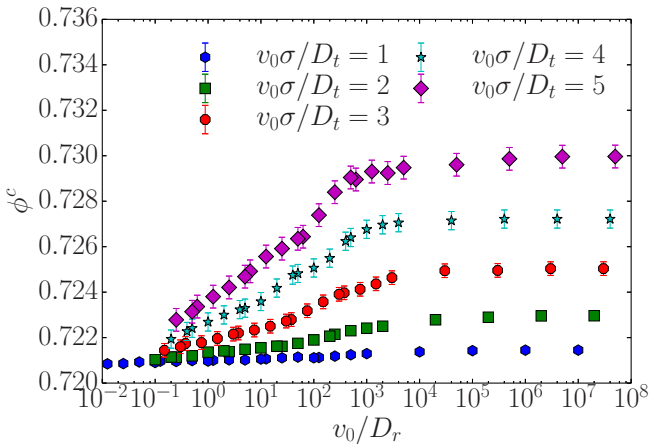

FIG. 9. Critical packing fraction $\phi^c(v_0, D_r)$ as a function of persistence length $\ell_p = v_0/D_r$ for various self-propulsion speeds v_0 as labeled.

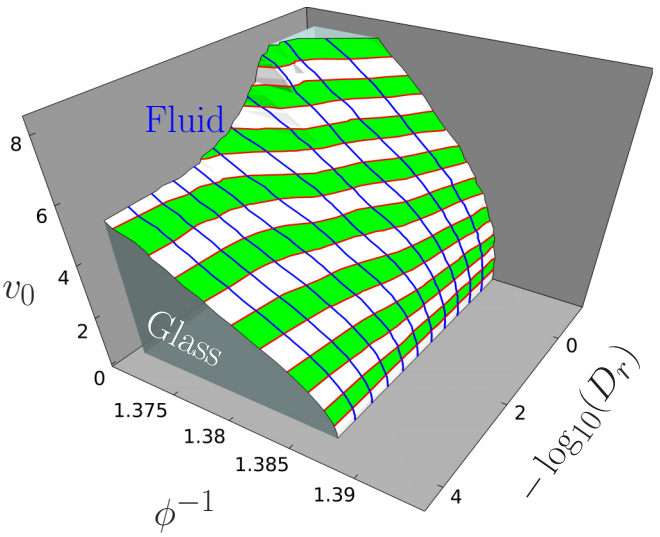

FIG. 10. MCT glass-transition surface for hard-disk ABPs, as estimated from power-law fits of the structural relaxation time. The gray shaded area below the surface is the glassy region.

diffusion coefficient shifts the transition to larger v_0. In particular, as $D_r \to \infty$, the glass-transition lines approach a vertical line in the (ϕ, v_0) plane, i.e., become independent of v_0 and identical to the passive ϕ^c. The functional form of the $v_0^c(\phi^c)$ curves in the window that is shown in Fig. 8 is well described by a square-root law. In other words, the self-propulsion velocity causes a quadratic enhancement in the glass-transition density. This might be expected based on the symmetry argument that the dynamics of the system should not change under the transformation $v_0 \mapsto -v_0$.

Figure 9 demonstrates the role of the persistence length in changing the glass transition. Here the transition points ϕ^c obtained by power-law extrapolations are shown for various fixed v_0 as functions of ℓ_p. In agreement with the discussion above, the curves for different v_0 separate at large ℓ_p. At fixed persistence length, stronger self-propulsion is more effective in shifting the glass transition to higher densities. As ℓ_p approaches zero, the glass-transition point of the passive system is recovered for all v_0. Interestingly, the point where the activity dependence of the glass transition starts being significant is close to the point where $\ell_p \approx \ell_c \approx 0.1\sigma$, i.e., the cage size.

For large ℓ_p, the extrapolated values of the critical density ϕ^c approach D_r-independent limiting values. A proper analysis of this regime is difficult due to the fact that the limits $t \to \infty$ and $\tau_r \to \infty$ do not commute. We have checked that our fits include at least some points where $\tau > \tau_r$ for the values shown in Fig. 9, but for $v_0/D_r \gg 10^4$ numerical instabilities make it impossible to rule out a crossover from one apparent divergence seen for observation times up to $t \sim \tau_r$ to another one at even larger times. The ϕ^c shown in Fig. 9 certainly correspond to the experimentally relevant effective glass-transition point.

Figure 10 summarizes the estimated glass-transition points of the MCT transition of active hard disks as a critical surface in the parameter space spanned by $(1/\phi, \log_{10}(1/D_r), v_0)$. This choice is motivated by a recent study of self-propelled cells in a Voronoi fluid model by Bi *et al.* [6]. In this model, a self-adhesion parameter p plays the role of an inverse density. In Ref. [6], an active-glass diagram was conjectured that includes two limiting shapes for $D_r \to 0$ and $D_r \to \infty$ with a crossover between them around $D_r = 1$. The numerical results shown in Fig. 10 are in good agreement with the conjecture by Bi *et al.* [6] over the range of D_r shown. A glass-transition surface emerges that extends from a limiting line in the $(v_0, 1/\phi)$ plane at $D_r = 0$. This is the glass transition given by the bifurcation points of Eq. (25). The transition surface bends upward to higher v_0 as D_r increases beyond $D_r \approx 0.01$. From the discussion above, one expects the glass-transition surface to bend over to a vertical plane as $D_r \to \infty$ (i.e., to the right of Fig. 10). This aspect is somewhat different from what was suggested in Ref. [6] for the self-propelled Voronoi fluid. Note that the dependence on D_r is quite unexpected from the traditional MCT viewpoint, since it is a parameter that characterizes the short-time motion of the particles and usually such parameters drop from the equations that determine the MCT transition points [56]. The reappearance of D_r through the extra term $\boldsymbol{\omega}_R \boldsymbol{S}_0(\vec{q}\,)$ in Eq. (26b) indicates that the active-glass transition within MCT is quite different from the MCT transitions that have been studied so far.

To characterize the glassy structure, we show in Fig. 11(a) the nonergodicity parameters of the positional-density correlation functions $F_{00}(\vec{q}\,)$ for different v_0 at fixed packing fraction. The passive case $v_0 = 0$ is included for reference; it shows the known features of $F_{00}(\vec{q}\,)$: The nonergodicity parameters oscillate in phase with the static structure factor. They are most pronounced around $q\sigma \approx 7$, indicating that the glass is stiffest with respect to density fluctuations of wavelengths comparable to the particle size.

Increasing v_0, the nonergodicity parameters decrease for all q. Thus, active driving renders the glass mechanically softer at fixed density. The effect, however, is minor: For most q, the values for $v_0 = 5D_t/\sigma$ are less than 10% smaller compared to the passive case. The decrease in mechanical stiffness of the glass with increasing activity might be counterintuitive: With increasing Péclet number Pe, the effective pressure of the system according to its low-density description increases [78]. Such an increase in pressure might, by analogy to the

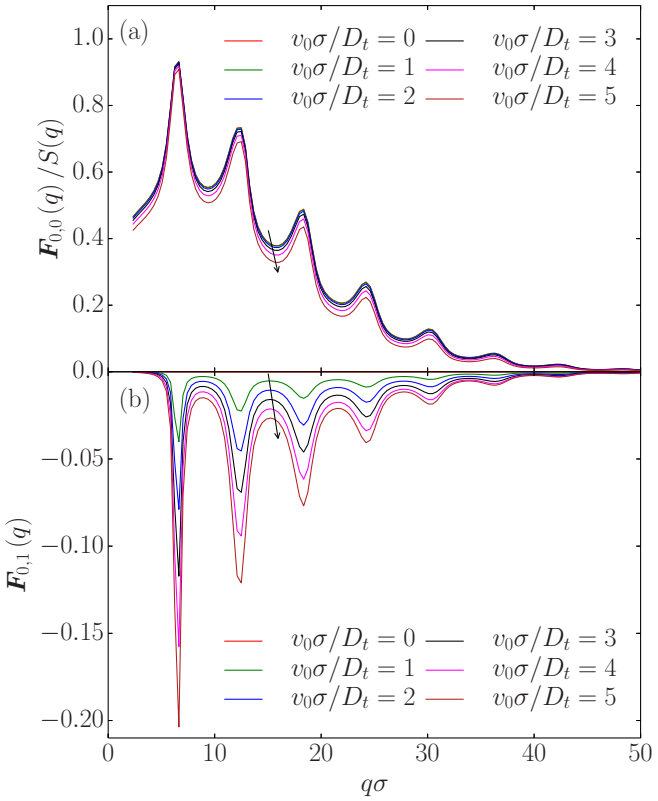

FIG. 11. (a) Nonergodicity parameters $F_{00}(\vec{q}\,) = \lim_{t\to\infty} \Phi_{00}(\vec{q},t)$ of the transient density correlation functions, obtained from Eqs. (26). Curves from top to bottom correspond to increasing self-propulsion velocity (as labeled) at fixed packing fraction $\phi = 0.727$ and $D_r = 1D_t/\sigma^2$. (b) Nonergodicity parameters $F_{01}(\vec{q}\,)$ of the orientation-translation coupling.

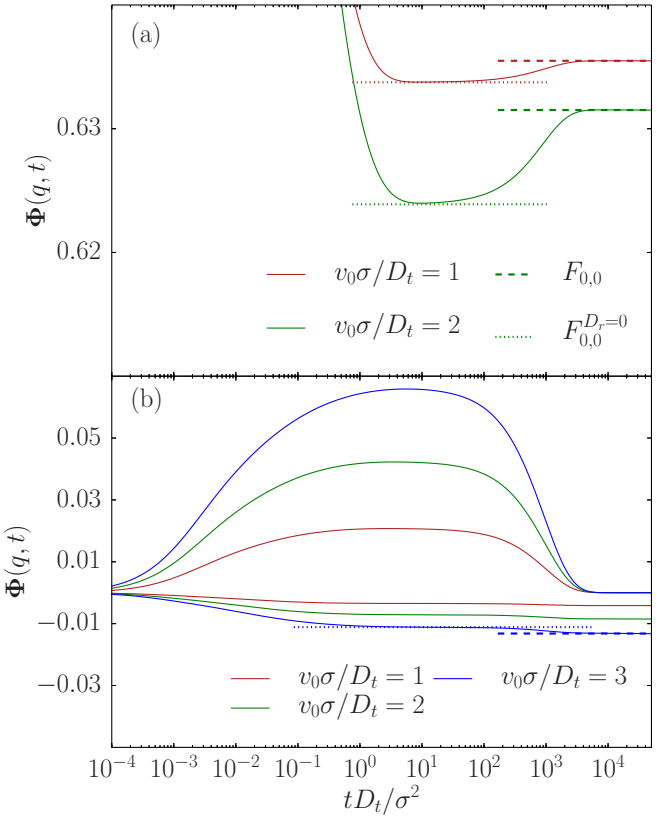

FIG. 12. Density correlator $\mathbf{\Phi}_{0,0}(q,t)$ for $q\sigma = 8$ (solid lines) as a function of time for a packing fraction $\phi = 0.727 > \phi^c$ and different velocities as labeled, for the case $D_r = 1/1000 D_t/\sigma^2$. The dashed and dotted lines correspond to the nonergodicity parameters at finite and zero rotational diffusion, Eqs. (26b) and (25), respectively.

passive system, be expected to cause an increase in mechanical stiffness. This shows that active forces act quite differently from thermodynamic ones at the glass transition.

There is an interesting observation regarding the off-diagonal components of $\boldsymbol{F}(\vec{q}\,)$: While $F_{l0}(\vec{q}\,) = 0$ for all $l \neq 0$, due to the presence of the hopping term proportional to $l^2 D_r$, the MCT equations admit solutions where $F_{0l}(\vec{q}\,) \neq 0$ for all l. In particular, $F_{01}(\vec{q}\,) \neq 0$, as shown in Fig. 11(b). For the reference frame chosen in our discussion, the values of $F_{01}(\vec{q}\,)$ are negative and real; this is consistent with the notion that there persists an anticorrelation between density fluctuations along the y direction and initial orientational fluctuations along the x direction. Note that the sign and real valuedness of $F_{01}(\vec{q}\,)$ are not invariant under rotations of the coordinate system. Apart from this, the $F_{01}(\vec{q}\,)$ show behavior that is qualitatively similar to the one seen in $F_{00}(\vec{q}\,)$: Oscillations are dictated by those in the equilibrium static structure factor and the strongest contribution comes from nearest-neighbor cage distances. In other words, the active glass keeps infinite memory not only in the translational degrees of freedom, but also in the coupling of orientations to translations, driven by fluctuations on the particle length scale. Loosely speaking, an initial orientation fluctuation leaves its fingerprint in the positions in the glass, while of course an initial density fluctuation does not affect the later orientation fluctuations.

The nonergodicity parameters discussed above are the values attained by the transient density correlation functions for large times, i.e., $D_t t/\sigma^2 \gg 1$ and in particular $D_r t \gg 1$. In the case of strongly persistent motion $D_r \ll D_t/\sigma^2$, an intermediate time window opens where $\sigma^2/D_t \ll t \ll 1/D_r$, i.e., for times large compared to the free diffusion time, but small compared to the time scale of reorientations. The effect of this additional time window is highlighted by Fig. 12: The density correlation functions approach a plateau in this regime that is given by the $D_r = 0$ glass transition (25). At $D_r t = 1$, an exponential crossover is seen from this plateau to a plateau given by the augmented equation for $D_r \neq 0$, Eq. (26b). This plateau depends on D_r, even if the MCT memory kernel does not, because in Eq. (26b) there appears an integral over the full correlator. Note that this radically changes the scaling laws known from standard MCT: In the passive case, the final plateau in the ideal glass is approached by a slow power law, the MCT critical law t^{-a} (with a nontrivial exponent $0 < a < 1/2$). In the present case, this critical decay is only seen in the approach to the first plateau. Hence the small-D_r case displays the crossover from the standard MCT glass to an active glass governed by details of the short-time motion. The ABPs with small rotational diffusivity could thus serve as an interesting model system to study the differences between two kinds of glasses.

V. CONCLUSION

We have developed a mode-coupling theory of the glass transition of active Brownian particles for the special case of spherically symmetric steric interactions. In contrast to prior approaches, we treat both the translational and reorientational degrees of freedom of the ABP model explicitly in the theory. This allows us to cover the full parameter range of self-propulsion velocities v_0 and persistence lengths $\ell_p = v_0/D_r$. With a typical particle size σ, these parameters correspond to the dimensionless swim Péclet number $\mathrm{Pe}_t = v_0\sigma/D_t$ and the reorientation Péclet number $\mathrm{Pe}_r = v_0\sigma/D_{\mathrm{eff}} = \sigma/\ell_p$ introduced earlier [39].

While at low densities the activity-induced dynamics is controlled by a single Péclet number only, $\mathrm{Pe} = \mathrm{Pe}_t/\mathrm{Pe}_r = v_0^2/D_rD_t$, we show that the high-density dynamics depends on both Pe_t and Pe_r separately. This arises because transient caging of particles imposes the average cage size ℓ_c as an additional length scale that interferes with the persistence length. Our results suggest the extension of studies of ABPs with various rotational relaxation times in order to explore the relation between the caging length and the persistence length in more detail.

Activity shifts the glass transition once the persistence length of swimming exceeds the cage size $\ell_p \gtrsim \ell_c$. The ABP MCT predicts a surface of idealized glass transitions in the parameter space spanned by the packing fraction, the persistence length, and the self-propulsion velocity (ϕ,ℓ_p,v_0). This surface does not collapse onto a single line in the (ϕ,Pe) plane as predicted by theories that start from a coarse-grained description of the orientational degrees of freedom. Genuine nonequilibrium features can arise once $\ell_p \approx \ell_c$, as seen, e.g., in the nonmonotonic decay of density fluctuations that indicates the joint effect of diffusive relaxation and persistent active motion. Our results may thus be taken as an indication that the mapping of the glassy dynamics of ABPs onto that of a near-equilibrium system should proceed with care.

The effects of active driving on the glassy dynamics are intuitive: Self-propulsion enhances structural relaxation, but only if it is persistent enough. Above a critical packing fraction $\phi^c(v_0,D_r)$, structural relaxation by the MCT mechanism becomes ineffective, and for densities above ϕ^c, a glassy state is reached. The features of this glass transition are in agreement with earlier simulation studies of the three-dimensional analog of the hard-disk ABP model [23]. Qualitatively, the predicted ABP MCT glass transition also matches the one that was estimated from earlier simulations of a self-propelled Voronoi fluid model [6]; this extends a qualitative analogy found in the passive case [79].

That the glass transition persists under finite activity is not *a priori* clear. A different scenario arises, for example, for shear-driven passive colloidal suspensions where MCT predicts the glass transition to vanish for arbitrarily weak driving [80]. This emphasizes that there are qualitatively different ways of driving a dense system out of equilibrium. Note, however, that according to our numerical results, the glass transition surface is a smooth surface around $v_0 = 0$; in particular, any small activity just at the passive glass transition will destroy the glass. This holds even in the case $D_r = 0$, i.e., if each particle maintains its randomly chosen initial propulsion direction forever. Compare this with the application of MCT to active microrheology of passive suspensions, i.e., the case of a single persistently driven particle in a bath of passive ones [73]: There it was found that a finite force threshold needs to be overcome to delocalize the driven particle. This threshold was associated with the strength of nearest-neighbor cages. It appears that collective driving of all particles allows one to collectively break such cages so that the force required to do so by a single particle approaches zero.

In the glass, density-density correlation functions $S_{00}(\vec{q},t)$ do not decay to zero, but to a finite long-time limit. This finite nonergodicity parameter quantifies the overlap of an initial positional-density fluctuation after infinitely long propagation with the positional-density fluctuations themselves. Similarly, a nonzero long-time limit emerges for $S_{0l}(\vec{q},t)$: Also the infinitely long propagated orientational fluctuations are required to determine the statistics of positional fluctuations in the glass. In this sense, the active glass keeps a memory of both initial positions and initial orientations.

The passive glass according to MCT is characterized by quantities that do not depend on the parameters determining the short-time motion; for a passive Brownian hard-sphere system, the short-time diffusivities D_t and D_r are irrelevant in the glass. This is no longer true for the active glass: Here the equation that determines the MCT glass transition depends on the integral of the correlation function and thus on the details of short-time diffusion in principle. In this sense, the active glass is qualitatively different from the passive one. Loosely speaking, while one can think of the passive glass as being determined by static long-time limits, the active glass is much more akin to a nonequilibrium dynamical balance.

Our ABP MCT is based on the integration-through-transients formalism and thus focuses on the calculation of so-called transient correlation functions that are formed with the full nonequilibrium dynamics but averaged using the equilibrium Boltzmann weight. These correlation functions are natural starting points for the calculation of nonequilibrium averages of, in principle, arbitrary observables within ITT.

ACKNOWLEDGMENTS

We acknowledge funding from Deutsche Forschungsgemeinschaft, as part of the Special Priority Programme SPP 1726 "Microswimmers" (Project No. Vo 1270/7). The authors gratefully acknowledge the computing time granted by the John von Neumann Institute for Computing and provided on the supercomputer JURECA [81] at Jülich Supercomputing Centre, under Project No. HKU26. We thank T. Franosch, T. Kranz, and R. Schilling for helpful discussions and A. Meyer for a critical reading of the manuscript.

APPENDIX A: DERIVATION OF THE MCT VERTEX

We briefly summarize the MCT approximation to the memory kernel. For convenience, we introduce the shorthand notation $(\vec{q}_1,l_1) \equiv 1$.

After inserting the projector $\mathcal{P}_2$ onto the two-point density fluctuations (20) to both sides of the reduced time-evolution

operator that appears in the memory kernel (18), one gets

$$m_{ll'}(\vec{q},t) \approx \sum_{\substack{1,2,3,4\\1',2',3',4'}} \langle \delta\varrho_l^*(\vec{q}\,)\,\Omega_T^\dagger\,\mathcal{Q}\,\delta\varrho_1\delta\varrho_2\rangle \chi_{121'2'} \times \langle \delta\varrho_{1'}^*\delta\varrho_{2'}^* e^{\mathcal{Q}\Omega_T^\dagger \mathcal{Q}' \mathcal{Q}t}\delta\varrho_{3'}\delta\varrho_{4'}\rangle \times \chi_{3'4'34}\langle \delta\varrho_3^*\delta\varrho_4^*\,\mathcal{Q}\,\Omega_T^\dagger\,\delta\varrho_{l'}(\vec{q}\,)\rangle. \tag{A1}$$

In the following, summation over repeated inner indices will be implied.

The next approximation consists of two intertwined steps, as outlined in the main text: factorization of the four-point correlation functions and replacement of the projected dynamics with the full one. (Either step performed alone will give undesirable results.) Consistent with the factorization (21), the normalization of $\mathcal{P}_2$ is chosen as $\chi_{121'2'} \approx (1/2)S_{11'}^{-1}S_{22'}^{-1}$.

The expressions to the left and to the right of the dynamical four-point function in Eq. (A1) define the vertices $\mathcal{W}^\dagger$ and $\mathcal{W}$. Their evaluation is straightforward, but there appears a static three-point density correlation function. In the absence of a well-established expression, we use the convolution approximation to express this three-point average in terms of the static structure factors

$$\langle \delta\varrho_1^*\delta\varrho_2\delta\varrho_3\rangle \approx \delta_{\vec{q}_1,\vec{q}_2+\vec{q}_3}\delta_{l_1,l_2+l_3}\boldsymbol{S}_1\boldsymbol{S}_2\boldsymbol{S}_3/\sqrt{N}. \tag{A2}$$

This is the two-dimensional analog of the approximation used in previous MCT for nonspherical molecules in 3D [76].

The contribution arising from the equilibrium dynamics to $\Omega_T^\dagger$ evaluates to a straightforward generalization of the MCT vertex of passive spherical particles [56,57],

$$\begin{aligned}\langle \delta\varrho_1^*\,\Omega_{\rm eq}^\dagger\,\mathcal{Q}\,\delta\varrho_2\delta\varrho_3\rangle &= -\frac{D_t}{\sqrt{N}}\delta_{\vec{q}_1-\vec{q}_2,\vec{q}_3}[(\vec{q}_1\cdot\vec{q}_2)S_{l_1-l_2,l_3}(q_3)+(\vec{q}_1\cdot\vec{q}_3)S_{l_1-l_3,l_2}(q_2)] + \langle \delta\varrho_1^*\,\Omega_{\rm eq}^\dagger\,\delta\varrho_{1'}\rangle S_{1'1'}^{-1}(\vec{q}_1)\langle \delta\varrho_{1'}^*\delta\varrho_2\delta\varrho_3\rangle \\ &\approx -\frac{D_t}{\sqrt{N}}\delta_{1,2+3}[(\vec{q}_1\cdot\vec{q}_2)S_{33}+(\vec{q}_1\cdot\vec{q}_3)S_{22}-q^2S_{22}S_{33}] = \frac{\rho D_t}{\sqrt{N}}\delta_{1,2+3}S_{22}S_{33}[(\vec{q}_1\cdot\vec{q}_2)c_{22}+(\vec{q}_1\cdot\vec{q}_3)c_{33}],\end{aligned} \tag{A3}$$

where we have used $\boldsymbol{S}^{-1} = \mathbf{1} - \rho\boldsymbol{c}$ to define the direct correlation function $c_{ll'}(q)$. Note that $c_{00}(q) \equiv c(q)$ is the only nonvanishing contribution to $\boldsymbol{c}(q)$.

To calculate the contribution that arises from $\delta\Omega^\dagger$, first consider

$$\begin{aligned}\langle \delta\varrho_1^*\,\delta\Omega^\dagger\,\delta\varrho_2\delta\varrho_3\rangle &= \frac{v_0}{2N^{3/2}}\sum_{jkm}\langle e^{-i\vec{q}_1\cdot\vec{r}_j - il_1\theta_j}\begin{pmatrix} e^{i\theta_k}+e^{-i\theta_k} \\ -ie^{i\theta_k}+ie^{-i\theta_k}\end{pmatrix}^T\cdot[i\vec{q}_2 e^{i\vec{q}_2\cdot\vec{r}_k+il_2\theta_k}e^{i\vec{q}_3\cdot\vec{r}_m+il_3\theta_m}+\{2\leftrightarrow 3\}] \\ &= \frac{iv_0}{2}\vec{q}_2\cdot\begin{pmatrix}1 & 1\\ -i & i\end{pmatrix}\cdot\begin{pmatrix}\langle\delta\varrho_1^*\delta\varrho_{2^+}\delta\varrho_3\rangle\\ \langle\delta\varrho_1^*\delta\varrho_{2^-}\delta\varrho_3\rangle\end{pmatrix}+\{2\leftrightarrow 3\},\end{aligned} \tag{A4}$$

where $\delta\varrho_{2^\pm} = \delta\varrho_{l_2\pm1}(\vec{q}_2)$. The contribution to the vertex thus yields, with $\mathcal{Q} = 1-\mathcal{P}$ and setting $\boldsymbol{T} = \left(\begin{smallmatrix}1 & 1\\ -i & i\end{smallmatrix}\right)$,

$$\langle \delta\varrho_1^*\,\delta\Omega^\dagger\,\mathcal{Q}\,\delta\varrho_2\delta\varrho_3\rangle = \frac{iv_0}{2}\left[\vec{q}_2\cdot\boldsymbol{T}\cdot\begin{pmatrix}\langle\delta\varrho_1^*\delta\varrho_{2^+}\delta\varrho_3\rangle\\ \delta\varrho_1^*\delta\varrho_{2^-}\delta\varrho_3\rangle\end{pmatrix}+\{2\leftrightarrow 3\}-\vec{q}_1\cdot\boldsymbol{T}\cdot\begin{pmatrix}S_{11}S_{1^-1^-}^{-1}\langle\delta\varrho_{1^-}^*\delta\varrho_2\delta\varrho_3\rangle\\ S_{11}S_{1^+1^+}^{-1}\langle\delta\varrho_{1^+}^*\delta\varrho_2\delta\varrho_3\rangle\end{pmatrix}\right]. \tag{A5}$$

With the aid of the convolution approximation this can be written in the form

$$\langle \delta\varrho_1^*\,\delta\Omega^\dagger\,\delta\varrho_2\delta\varrho_3\rangle \approx \frac{iv_0}{2\sqrt{N}}\left[\vec{q}_2\cdot\boldsymbol{T}\cdot\begin{pmatrix}S_{11}S_{2^+2^+}S_{33}\delta_{1^-,2+3}\\ S_{11}S_{2^-2^-}S_{33}\delta_{1^+,2+3}\end{pmatrix}+\vec{q}_3\cdot\boldsymbol{T}\cdot\begin{pmatrix}S_{11}S_{22}S_{3^+3^+}\delta_{1^-,2+3}\\ S_{11}S_{22}S_{3^-3^-}\delta_{1^+,2+3}\end{pmatrix}-\vec{q}_1\cdot\boldsymbol{T}\cdot\begin{pmatrix}S_{11}S_{22}S_{33}\delta_{1^-,2+3}\\ S_{11}S_{22}S_{33}\delta_{1^+,2+3}\end{pmatrix}\right]. \tag{A6}$$

Using $\vec{q}\cdot\boldsymbol{T} = q(e^{-i\vartheta_q}, e^{i\vartheta_q})^T$, one arrives at the form given in Eq. (23).

The nonequilibrium contribution to the vertex $\mathcal{W}$ vanishes. This follows from observing that $\delta\Omega^\dagger\,\delta\varrho_1$ lies in the subspace spanned by $\delta\varrho_{1^+}$ and $\delta\varrho_{1^-}$ and hence $\mathcal{Q}\,\delta\Omega^\dagger\,\delta\varrho_1 = 0$.

The final form of the MCT memory equation given in Eq. (22) follows from replacing, in the thermodynamic limit, $(1/V)\sum_{\vec{k}} \mapsto [1/(2\pi)^2]\int d\vec{k}$.

APPENDIX B: NUMERICAL ALGORITHM

To solve the ABP MCT time-evolution equations, we extend the standard algorithm used for MCT equations in the passive case [82]. It is based on the expectation that the solutions become slowly varying functions of time such that for long times, the derivatives of the correlation functions become small. This allows us to adopt a decimation procedure by which the integration domain is discretized in blocks (numbered $b = 0,\ldots,B-1$) of equidistant time steps (with fixed number per block), starting with step size h_0 and doubling the time step from block to block, $h_b = h_0 2^b$. Within each block, the equations can be solved by a simple backward Euler method. The integration time steps within each block are given by $t_i^{(b)} = ih_b$ and we abbreviate $f(t_i) \equiv f_i$.

Our algorithm applies to equations of the form

$$\partial_t \boldsymbol{S}(t) = -\boldsymbol{A}\cdot\boldsymbol{S}(t) - \int_0^t dt' \boldsymbol{m}(t-t') \cdot[\partial_{t'}\boldsymbol{S}(t') + \boldsymbol{B}\cdot\boldsymbol{S}(t')], \tag{B1}$$

with $\boldsymbol{S}(0) \equiv \boldsymbol{S}_0$. This equation can be recast as

$$\partial_t \bar{\boldsymbol{S}}(t) = -\bar{\boldsymbol{A}}\cdot\boldsymbol{S}(t) - \int_0^t dt' \boldsymbol{m}(t-t')\cdot\partial_{t'}\bar{\boldsymbol{S}}(t'), \tag{B2a}$$

$$\partial_t \boldsymbol{S}(t) = \partial_t \bar{\boldsymbol{S}}(t) - \boldsymbol{B}\cdot\boldsymbol{S}(t), \tag{B2b}$$

with $\bar{\boldsymbol{S}}(0) = \boldsymbol{S}_0$ and $\bar{\boldsymbol{A}} = \boldsymbol{A} - \boldsymbol{B}$. The introduction of the auxiliary function $\bar{\boldsymbol{S}}(t)$ is the essential difference from previous numerical algorithms for MCT equations. The following steps are standard in this context.

To discretize Eqs. (B2), backward finite differences are used for the time derivatives $\partial_t \boldsymbol{S}_i = [(3/2)\boldsymbol{S}_i - 2\boldsymbol{S}_{i-1} + (1/2)\boldsymbol{S}_{i-2}]/h_b$, assuming that the first few points in each given block are known. [The latter is ensured in block $b = 0$ by a calculation of an appropriate short-time expansion of $\boldsymbol{S}(t)$.]

To deal with the convolution integral in Eq. (B2a), it is useful to define so-called moments

$$d\bar{\boldsymbol{S}}_i = \frac{1}{h_b}\int_{t_{i-1}}^{t_i} \bar{\boldsymbol{S}}(t)dt, \quad d\boldsymbol{m}_i = \frac{1}{h_b}\int_{t_{i-1}}^{t_i} \boldsymbol{m}(t)dt. \tag{B3}$$

This allows us to approximate

$$\int_0^t dt' \boldsymbol{m}(t-t')\cdot\partial_{t'}\bar{\boldsymbol{S}}(t') \approx \boldsymbol{m}_{i-\bar{\imath}}\cdot\bar{\boldsymbol{S}}_{\bar{\imath}} - \boldsymbol{m}_i\cdot\boldsymbol{S}_0 + \sum_{k=1}^{\bar{\imath}}[\boldsymbol{m}_{i-k+1} - \boldsymbol{m}_{i-k}]\cdot d\bar{\boldsymbol{S}}_k + \sum_{k=1}^{i-\bar{\imath}} d\boldsymbol{m}_k\cdot[\bar{\boldsymbol{S}}_{i-k+1} - \bar{\boldsymbol{S}}_{i-k}]. \tag{B4}$$

Here the convolution integral has been split at a time $t_{\bar{\imath}}$ roughly in the middle of the interval $\bar{\imath} = \lfloor i/2 \rfloor$ and the integrand was assumed to be slowly varying for $t \gtrsim t_{\bar{\imath}}$.

An essential feature of the MCT approximation is that $\boldsymbol{m}_i$ is a functional of $\boldsymbol{S}_i$. After discretization, Eqs. (B2) are thus recast as a set of implicit equations

$$\boldsymbol{S}_i = \boldsymbol{\mathcal{S}}_L^{-1}\cdot\left[\frac{3}{2h_b}\bar{\boldsymbol{S}}_i + \boldsymbol{\mathcal{S}}_R\right], \tag{B5a}$$

$$\bar{\boldsymbol{S}}_i = \bar{\boldsymbol{\mathcal{S}}}^{-1}\cdot(\boldsymbol{m}_i[\boldsymbol{S}_i]\cdot\bar{\boldsymbol{\mathcal{M}}} - \bar{\boldsymbol{\mathcal{I}}}_i), \tag{B5b}$$

where we have defined auxiliary matrices

$$\boldsymbol{\mathcal{S}}_L = \frac{3}{2h_b}\mathbf{1} + \boldsymbol{B}, \tag{B6a}$$

$$\boldsymbol{\mathcal{S}}_R = \frac{1}{h_b}\left[-2(\bar{\boldsymbol{S}}_{i-1} - \boldsymbol{S}_{i-1}) + \tfrac{1}{2}(\bar{\boldsymbol{S}}_{i-2} - \boldsymbol{S}_{i-2})\right], \tag{B6b}$$

$$\bar{\boldsymbol{\mathcal{S}}} = \frac{3}{2h_b}\mathbf{1} + \frac{3}{2h_b}\bar{\boldsymbol{A}}\cdot\boldsymbol{\mathcal{S}}_L^{-1} + d\boldsymbol{m}_1, \tag{B6c}$$

$$\bar{\boldsymbol{\mathcal{M}}} = \boldsymbol{S}_0 - d\bar{\boldsymbol{S}}_1 \tag{B6d}$$

and abbreviated the convolution sum as

$$\bar{\boldsymbol{\mathcal{I}}}_i = \frac{1}{h_b}\left[-2\bar{\boldsymbol{S}}_{i-1} + \tfrac{1}{2}\bar{\boldsymbol{S}}_{i-2}\right] + \boldsymbol{A}\cdot\boldsymbol{\mathcal{S}}_L^{-1}\cdot\boldsymbol{\mathcal{S}}_R + \boldsymbol{m}_{i-\bar{\imath}}\cdot\bar{\boldsymbol{S}}_{\bar{\imath}} - \boldsymbol{m}_{i-1}\cdot d\bar{\boldsymbol{S}}_1 - d\boldsymbol{m}_1\cdot\bar{\boldsymbol{S}}_{i-1} + \sum_{k=2}^{\bar{\imath}}[\boldsymbol{m}_{i-k+1} - \boldsymbol{m}_{i-k}]\cdot d\bar{\boldsymbol{S}}_k + \sum_{k=2}^{i-\bar{\imath}} d\boldsymbol{m}_k\cdot[\bar{\boldsymbol{S}}_{i-k+1} - \bar{\boldsymbol{S}}_{i-k}]. \tag{B6e}$$

This quantity can be evaluated based on function values at grid points t_j with $j < i$ only; Eqs. (B5) are then solved iteratively to determine $\boldsymbol{S}(t)$ and consequently $\boldsymbol{m}(t)$ and $\bar{\boldsymbol{S}}(t)$ at $t = t_i$.

Once a block b is completed, a decimation procedure transfers the discretized solutions to the first half of the next block $b+1$. For the correlation functions and the memory kernel, this is done by simple injection $\boldsymbol{S}_i^{(b+1)} \leftarrow \boldsymbol{S}_{2i}^{(b)}$. Note that this keeps $\boldsymbol{S}_0 \equiv \boldsymbol{S}(0)$ in all blocks. The moments can be decimated without further loss of accuracy, $d\boldsymbol{S}_i^{(b+1)} \leftarrow [d\boldsymbol{S}_{2i-1}^{(b)} + d\boldsymbol{S}_{2i}^{(b)}]/2$.

Solutions are calculated on a regular wave-number grid. It is then convenient to rewrite the wave-vector integral that appears in the MCT memory kernel, in terms of a double integral in the space of wave numbers. In 2D, this introduces a singular Jacobian [58]

$$\int \frac{d^2k}{(2\pi)^2}\delta_{\vec{q},\vec{k}+\vec{p}} = \frac{1}{(2\pi)^2}\int_0^\infty dk \int_{|q-k|}^{q+k} dp \times \frac{kp}{\sqrt{4q^2k^2 - (q^2+k^2-p^2)^2}}. \tag{B7}$$

To treat this pole without significant loss of precision and performance, we use a fifth-order open extended Newton-Cotes formula (as derived in Ref. [83])

$$\int_{q_1}^{q_N} f(q)dq = h_q\left[\tfrac{55}{24}f_2 - \tfrac{1}{6}f_3 + \tfrac{11}{8}f_4 + \cdots + \tfrac{11}{8}f_{N-3} - \tfrac{1}{6}f_{N-2} + \tfrac{55}{24}f_{N-1}\right], \tag{B8}$$

where the ellipsis abbreviates terms with unit coefficients and $f_i = f(q_i)$ for a set of equidistant integration points q_i in the interval $[q_1, q_N]$. The use of this formula improves the *ad hoc* discretization scheme used in previous MCT calculations of two-dimensional hard disks [58].

[1] M. Poujade, E. Grasland-Mongrain, A. Hertzog, J. Jouanneau, P. Chavrier, B. Ladoux, A. Buguin, and P. Silberzan, Proc. Natl. Acad. Sci. USA **104**, 15988 (2007).

[2] L. Petitjean, M. Reffay, E. Grasland-Mongrain, M. Poujade, B. Ladoux, A. Buguin, and P. Silberzan, Biophys. J. **98**, 1790 (2010).

[3] X. Trepat, M. R. Wasserman, T. E. Angelini, E. Millet, D. A. Weitz, J. P. Butler, and J. J. Fredberg, Nat. Phys. **5**, 426 (2009).
[4] T. E. Angelini, E. Hannezo, X. Trepat, J. J. Fredberg, and D. A. Weitz, Phys. Rev. Lett. **104**, 168104 (2010).
[5] K. D. Nnetu, M. Knorr, J. Käs, and M. Zink, New J. Phys. **14**, 115012 (2012).
[6] D. Bi, X. Yang, M. C. Marchetti, and M. L. Manning, Phys. Rev. X **6**, 021011 (2016).
[7] B. Fabry, G. N. Maksym, J. P. Butler, M. Glogauer, D. Navajas, and J. J. Fredberg, Phys. Rev. Lett. **87**, 148102 (2001).
[8] P. Bursac, G. Lenormand, B. Fabry, M. Oliver, D. A. Weitz, V. Viasnoff, J. P. Butler, and J. J. Fredberg, Nat. Mater. **4**, 557 (2005).
[9] E. H. Zhou, X. Trepat, C. Y. Park, G. Lenormand, M. N. Oliver, S. M. Mijailovich, C. Hardin, D. A. Weitz, J. P. Butler, and J. J. Fredberg, Proc. Natl. Acad. Sci. USA **106**, 10632 (2009).
[10] S. Wang, T. Shen, and P. G. Wolynes, J. Chem. Phys. **134**, 014510 (2011).
[11] F. Peruani, J. Starruß, V. Jakovljevic, L. Søgaard-Andersen, A. Deutsch, and M. Bär, Phys. Rev. Lett. **108**, 098102 (2012).
[12] M. Sadati, N. T. Qazvini, R. Krishnan, C. Y. Park, and J. J. Fredberg, Differentiation **86**, 121 (2013).
[13] J.-A. Park *et al.*, Nat. Mater. **14**, 1040 (2015).
[14] A. Erbe, M. Zientara, L. Baraban, C. Kreidler, and P. Leiderer, J. Phys.: Condens. Matter **20**, 404215 (2008).
[15] L. Baraban, M. Tasinkevych, M. N. Popescu, S. Sanchez, S. Dietrich, and O. G. Schmidt, Soft Matter **8**, 48 (2012).
[16] J. Palacci, C. Cottin-Bizonne, C. Ybert, and L. Bocquet, Phys. Rev. Lett. **105**, 088304 (2010).
[17] I. Buttinoni, J. Bialké, F. Kümmel, H. Löwen, C. Bechinger, and T. Speck, Phys. Rev. Lett. **110**, 238301 (2013).
[18] G. Volpe, I. Buttinoni, D. Vogt, H.-J. Kümmerer, and C. Bechinger, Soft Matter **7**, 8810 (2011).
[19] I. Theurkauff, C. Cottin-Bizonne, J. Palacci, C. Ybert, and L. Bocquet, Phys. Rev. Lett. **108**, 268303 (2012).
[20] A. Zöttl and H. Stark, J. Phys.: Condens. Matter **28**, 253001 (2016).
[21] M. C. Marchetti, Y. Fily, S. Henkes, A. Patch, and D. Yllanes, Curr. Opin. Colloid Interface Sci. **21**, 34 (2016).
[22] P. K. Ghosh, Y. Li, G. Marchegiani, and F. Marchesoni, J. Chem. Phys. **143**, 211101 (2015).
[23] R. Ni, M. A. C. Stuart, and M. Dijkstra, Nat. Commun. **4**, 2704 (2013).
[24] Y. Fily, S. Henkes, and M. C. Marchetti, Soft Matter **10**, 2132 (2013).
[25] H.-S. Kuan, R. Blackwell, L. E. Hough, M. A. Glaser, and M. D. Betterton, Phys. Rev. E **92**, 060501(R) (2015).
[26] L. Berthier and J. Kurchan, Nat. Phys. **9**, 310 (2013).
[27] L. Berthier, Phys. Rev. Lett. **112**, 220602 (2014).
[28] D. Levis and L. Berthier, Europhys. Lett. **111**, 60006 (2015).
[29] G. Szamel, E. Flenner, and L. Berthier, Phys. Rev. E **91**, 062304 (2015).
[30] R. Mandal, P. J. Bhuyan, M. Rao, and C. Dasgupta, Soft Matter **12**, 6268 (2016).
[31] M. Enculescu and H. Stark, Phys. Rev. Lett. **107**, 058301 (2011).
[32] J. Bialké, T. Speck, and H. Löwen, Phys. Rev. Lett. **108**, 168301 (2012).
[33] J. Bialké, H. Löwen, and T. Speck, Europhys. Lett. **103**, 30008 (2013).
[34] T. Speck, J. Bilaké, A. M. Menzel, and H. Löwen, Phys. Rev. Lett. **112**, 218304 (2014).
[35] J. Bialké, J. T. Siebert, H. Löwen, and T. Speck, Phys. Rev. Lett. **115**, 098301 (2015).
[36] M. E. Cates and J. Tailleur, Europhys. Lett. **101**, 20010 (2013).
[37] A. P. Solon, J. Stenhammar, R. Wittkowski, M. Kardar, Y. Kafri, M. E. Cates, and J. Tailleur, Phys. Rev. Lett. **114**, 198301 (2015).
[38] A. P. Solon, Y. Fily, A. Baskaran, M. E. Cates, Y. Kafri, M. Kardar, and J. Tailleur, Nat. Phys. **11**, 673 (2015).
[39] S. C. Takatori, W. Yan, and J. F. Brady, Phys. Rev. Lett. **113**, 028103 (2014).
[40] S. C. Takatori, R. De Dier, J. Vermant, and J. F. Brady, Nat. Commun. **7**, 10694 (2015).
[41] S. C. Takatori and J. F. Brady, Curr. Opin. Colloid Interface Sci. **21**, 24 (2016).
[42] W. Yan and J. F. Brady, Soft Matter **11**, 6235 (2015).
[43] W. Yan and J. F. Brady, J. Fluid Mech. **785**, R1 (2015).
[44] R. G. Winkler, A. Wysocki, and G. Gompper, Soft Matter **11**, 6680 (2015).
[45] A. Wysocki, R. G. Winkler, and G. Gompper, Europhys. Lett. **105**, 48004 (2013).
[46] T. F. F. Farage, P. Krinninger, and J. M. Brader, Phys. Rev. E **91**, 042310 (2015).
[47] C. Kurzthaler, S. Leitmann, and T. Franosch, Sci. Rep. **6**, 36702 (2016).
[48] Z. Preisler and M. Dijkstra, Soft Matter **12**, 6043 (2016).
[49] M. Han, J. Yan, S. Granick, and E. Luijten, Proc. Natl. Acad. Sci. USA **114**, 7513 (2017).
[50] S. Wang and P. G. Wolynes, J. Chem. Phys. **135**, 051101 (2011).
[51] T. F. F. Farage and J. M. Brader, arXiv:1403.0928.
[52] G. Szamel, Phys. Rev. E **93**, 012603 (2016).
[53] S. K. Nandi, R. Mandal, P. J. Bhuyan, C. Dasgupta, M. Rao, Nir. S. Gov, arXiv:1605.06073.
[54] S. K. Nandi, arXiv:1607.04478.
[55] S. K. Nandi and N. S. Gov, Soft Matter **13**, 7609 (2017).
[56] W. Götze, *Complex Dynamics of Glass-Forming Liquids* (Oxford University Press, New York, 2009).
[57] G. Szamel and H. Löwen, Phys. Rev. A **44**, 8215 (1991).
[58] M. Bayer, J. M. Brader, F. Ebert, M. Fuchs, E. Lange, G. Maret, R. Schilling, M. Sperl, and J. P. Wittmer, Phys. Rev. E **76**, 011508 (2007).
[59] H. Ding, M. Feng, H. Jiang, and Z. Hou, arXiv:1506.02754.
[60] D. Levis and L. Berthier, Phys. Rev. E **89**, 062301 (2014).
[61] E. Flenner, G. Szamel, and L. Berthier, Soft Matter **12**, 7136 (2016).
[62] G. Szamel, Phys. Rev. E **90**, 012111 (2014).
[63] U. M. B. Marconi and C. Maggi, Soft Matter **11**, 8768 (2015).
[64] Z. Sadjadi, M. R. Shaebani, H. Rieger, and L. Santen, Phys. Rev. E **91**, 062715 (2015).
[65] M. Feng and Z. Hou, Soft Matter **13**, 4464 (2017).
[66] C. Reichhardt and C. J. Olson Reichhardt, Soft Matter **10**, 7502 (2014).
[67] A. Sharma and J. M. Brader, J. Chem. Phys. **145**, 161101 (2016).
[68] G. Szamel, J. Chem. Phys. **127**, 084515 (2007).
[69] M. Baus and J.-L. Colot, J. Phys. C **19**, L643 (1986).
[70] W. Götze and L. Sjögren, J. Math. Anal. Appl. **195**, 230 (1995).
[71] T. Franosch and T. Voigtmann, J. Stat. Phys. **109**, 237 (2002).
[72] M. Fuchs and M. E. Cates, Faraday Discuss. **123**, 267 (2003).
[73] I. Gazuz, A. M. Puertas, T. Voigtmann, and M. Fuchs, Phys. Rev. Lett. **102**, 248302 (2009).

[74] T. Franosch, M. Fuchs, W. Götze, M. R. Mayr, and A. P. Singh, Phys. Rev. E **56**, 5659 (1997).
[75] S. Kämmerer, W. Kob, and R. Schilling, Phys. Rev. E **56**, 5450 (1997).
[76] R. Schilling and T. Scheidsteger, Phys. Rev. E **56**, 2932 (1997).
[77] R. Schilling, Phys. Rev. E **65**, 051206 (2002).
[78] J. Tailleur and M. E. Cates, Phys. Rev. Lett. **100**, 218103 (2008).
[79] C. Ruscher, J. Baschnagel, and J. Farago, Europhys. Lett. **112**, 66003 (2015).
[80] M. Fuchs and M. E. Cates, Phys. Rev. Lett. **89**, 248304 (2002).
[81] D. Krause and P. Thörnig, J. Large-Scale Res. Facilities **2**, A62 (2016).
[82] T. Voigtmann, Mode coupling theory of the glass transition in binary mixtures, Ph.D. thesis, TU München, 2003 .
[83] W. H. Press, S. A. Teukolsky, W. T. Vetterling, and B. P. Flannery, *Numerical Recipes*, 2nd ed. (Cambridge University Press, Cambridge, 1992).